Electronic structure of the S1 state in methylcobalamin: insight from CASSCF/MC-XQDPT2, EOM-CCSD, and TD-DFT calculations

ARTICLE *in* JOURNAL OF COMPUTATIONAL CHEMISTRY · MAY 2013

Impact Factor: 3.59 · DOI: 10.1002/jcc.23204 · Source: PubMed

8 AUTHORS, INCLUDING:

Neeraj Kumar
Pacific Northwest National Laboratory
14 PUBLICATIONS **131** CITATIONS
SEE PROFILE

Piotr Lodowski
University of Silesia in Katowice
47 PUBLICATIONS **383** CITATIONS
SEE PROFILE

Jesse Lutz
Durham University
12 PUBLICATIONS **163** CITATIONS
SEE PROFILE

Bryan M. Wong
University of California, Riverside
89 PUBLICATIONS **1,455** CITATIONS
SEE PROFILE

Electronic Structure of the S_1 State in Methylcobalamin: Insight from CASSCF/MC-XQDPT2, EOM-CCSD, and TD-DFT Calculations

Karina Kornobis,[a] Neeraj Kumar,[a] Piotr Lodowski,[b] Maria Jaworska,[b] Piotr Piecuch,*[c] Jesse J. Lutz,[c] Bryan M. Wong,[d] and Pawel M. Kozlowski*[a]

The methylcobalamin cofactor (MeCbl), which is one of the biologically active forms of vitamin B_{12}, has been the subject of many spectroscopic and theoretical investigations. Traditionally, the lowest-energy part of the photoabsorption spectrum of MeCbl (the so-called α/β band) has been interpreted as an $S_0 \rightarrow S_1$ electronic transition dominated by $\pi \rightarrow \pi^*$ excitations associated with the C=C stretching of the corrin ring. However, a more quantitative band-shape analysis of the α/β spectral region, along with circular dichroism (CD), magnetic CD, and resonance Raman data, has revealed the presence of a second electronic transition that involves the $Co{-}C_{Me}$ bond weakening. Conversely, the lowest-energy excitations based on transient absorption spectroscopy measurements have been interpreted as metal-to-ligand charge transfer (MLCT) transitions. To resolve the existing controversy about the interpretation of the S_1 state of MeCbl, calculations have been performed using two independent *ab initio* wavefunction-based methods. These include the modified variant of the second-order multiconfigurational quasi-degenerate perturbation theory (MC-XQDPT2), using complete active space self-consistent field orbitals, and the equation-of-motion coupled-cluster singles and doubles (EOM-CCSD) approach using restricted Hartree–Fock orbitals. It is shown that both *ab initio* methods provide a consistent description of the S_1 state as having an MLCT character. In addition, the performance of different types of functionals, including hybrid (B3LYP, MPW1PW91, TPSSh), generalized-gradient-approximation-type (GGA-type) (BP86, BLYP, MPWPW91), meta-GGA (TPSS), and range-separated (CAM-B3LYP, LC-BLYP) approaches, has been examined and the results of the corresponding time-dependent density functional theory calculations have been benchmarked against the MC-XQDPT2 and EOM-CCSD data. The hybrid functionals support the interpretation in which the S_1 state represents a $\pi \rightarrow \pi^*$ transition localized on corrin, while pure GGA, meta-GGA, and LC-BLYP functionals produce results consistent with the MLCT assignment. © 2013 Wiley Periodicals, Inc.

DOI: 10.1002/jcc.23204

Introduction

Derivatives of vitamin B_{12} (cyanocobalamin or CNCbl), such as the methylcobalamin (MeCbl) or adenosylcobalamin (AdoCbl) cofactors (Fig. 1), catalyze complex molecular transformations in which cleavage of the cobalt-carbon bond constitutes one of the key steps.[1–19] Both cofactors possess a complex manifold of electronically excited states that have been probed by various experimental techniques. Among them, the most widely used is photoabsorption (Abs) spectroscopy, resulting in spectra characterized by several prominent bands.[20–22] For typical cobalamins, these bands fall into the following four categories: (i) the α and β bands, which are a series of low to medium intensity transitions in the 420–600 nm region, (ii) the D and E bands, which are bands of low intensity in the 390–420 nm region, (iii) the γ band, which is the most intense photoabsorption peak in the 350–370 nm region, usually accompanied by a shoulder on the high-energy side, and (iv) the δ band, which is characterized by a low to medium intensity in the 300–330 nm region. The bands observed in the Abs spectra of cobalamins were named after their analogs in porphyrin spectra, since these α, β, γ, and δ bands are shared by both classes of metal complexes.[21,22]

Traditionally, the main photoabsorption features characterizing cobalamins have been interpreted as electronic transitions associated with the corrin ring,[23–25] which is a recurring structural motif in all B_{12} complexes. The evidence supporting this interpretation has been provided by studies on cobalt-free

[a] *K. Kornobis, N. Kumar, P. M. Kozlowski*
Department of Chemistry, University of Louisville, 2320 South Brook St., Louisville, Kentucky 40292
E-mail: pawel@louisville.edu
[b] *P. Lodowski, M. Jaworska*
Institute of Chemistry, University of Silesia, Szkolna 9, PL-40 006 Katowice, Poland
[c] *P. Piecuch, J. J. Lutz*
Department of Chemistry, Michigan State University, 578 S. Shaw Lane, East Lansing, Michigan 48824 E-mail: piecuch@chemistry.msu.edu
[d] *B. M. Wong*
Materials Chemistry Department, Sandia National Laboratories, Livermore, California 94551

Contract/grant sponsor: Office of Basic Energy Sciences, Office of Science, US Department of Energy (to PP); Contract/grant number: DE-FG02-01ER15228; Contract/grant sponsor: US Department of Energy's National Nuclear Security Administration; Contract/grant number: DE-AC04-94AL85000.

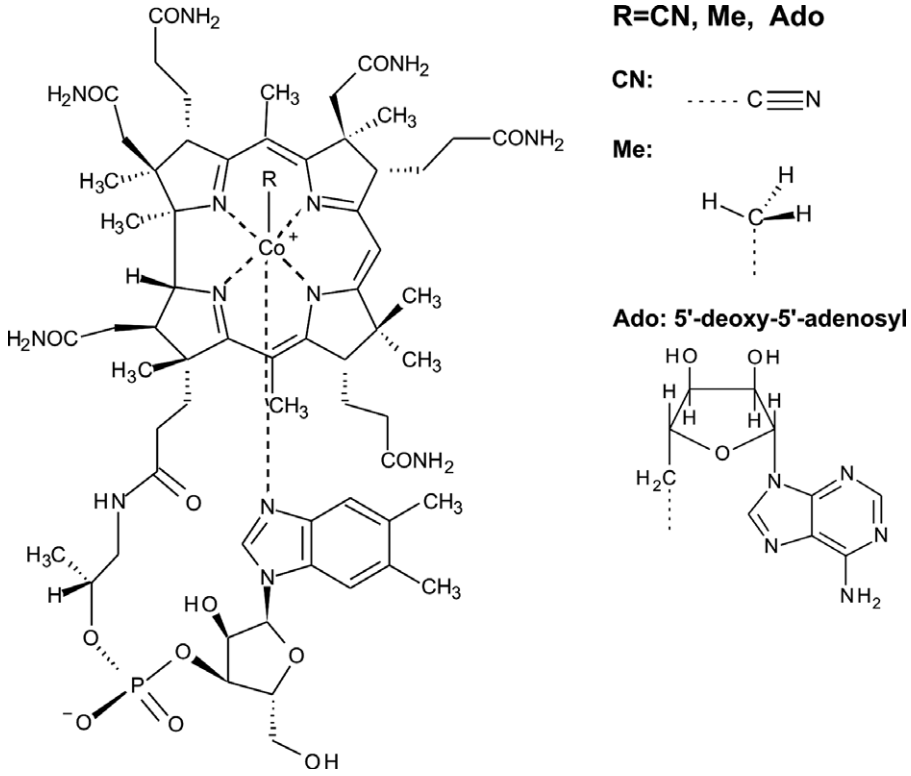

Figure 1. Molecular structure of vitamin B_{12} (CNCbl = cyanocobalamin, R = CN), methylcobalamin (R = Me), and adenosylcobalamin (R = Ado). The nucleotide loop is connected to C_{17} of the corrin ring.

corrin derivative,[26] where it has been shown that its Abs spectrum displays maxima in the visible region that coincide with those observed for aquocobamides. Subsequently, the spectroscopic studies have been extended to a variety of B_{12} derivatives which have revealed more subtle differences.[27–30] The systematic analysis of circular dichroism (CD), along with the Abs data for nonalkyl as well as alkyl cobalamins, has become the foundation for the classification of the corresponding electronic spectra as "normal" and "anomalous."[20] The latter spectral type has been attributed to MeCbl, and its primary manifestation is a decrease in intensity of the α band compared to the neighboring β band coupled with an intensity reduction of the γ band and its distribution among several similarly intense transitions in the UV region. In spite of the gradual changes in the Abs spectra of B_{12} derivatives induced by the substitution of the upper axial position by different ligands, the lower-energy α band has traditionally been characterized as a $\pi\rightarrow\pi^*$ excitation,[21,22] whereas the neighboring β region of the Abs spectrum has usually been interpreted as originating from a vibrational progression within a single electronic $S_0\rightarrow S_1$ transition. In other words, the α/β band has typically been interpreted as a superposition of the 0-0 and 0-1 components of the lowest-energy electronic $\pi\rightarrow\pi^*$ transition associated with the vibrational mode that primarily involves the C=C stretching of the corrin ring.[22]

Herein, it is important to draw attention to the results originating from time-dependent density functional theory (TD-DFT)[31–35] calculations in context of the interpretation of the energetically lowest $S_0\rightarrow S_1$ band in cobalamins described as $\pi\rightarrow\pi^*$ excitations within the corrin conjugation.[36–38] The early TD-DFT analyses based on the hybrid B3LYP functional[39,40] (which has been recommended as one of the most appropriate functionals to study bioinorganic molecules[41]) carried out for models of vitamin B_{12} have demonstrated that the lowest-energy photoabsorption band is associated with a single electronic transition.[36] The subsequent spectroscopic and computational studies reported by Brunold and coworkers[27] have resulted in the assignment of major spectral features and the generation of the experimentally validated electronic-structure description based on the Abs, CD, and magnetic CD (MCD) spectra. To explain the difference between the α/β regions of the "typical" and "unique" Abs spectra of cobalamins (note that the alternative terms "normal" and "anomalous" were used for these systems in the older studies[20]), a quantitative band-shape analysis for several molecular models was performed within the framework of time-dependent Heller theory and TD-DFT, where both nonalkyl and alkyl cobalamins were taken into consideration.[27] Based on TD-DFT/B3LYP computations, it was concluded[27] that the energetically lowest excited state can indeed be described as a $\pi\rightarrow\pi^*$ transition, in accordance with the original assignment[20–22] and several previous calculations.[23,25,36] However, some inconsistencies were noticed, when the assumption of a single electronic transition was applied to the lowest-energy band. In the case of CNCbl, it was concluded that the α/β part of the Abs spectrum in the visible region should result from the corrin-based HOMO-LUMO transition assigned as a $\pi\rightarrow\pi^*$ excitation.[27] For the α/β region of the MeCbl Abs spectrum, it was suggested[27] that

the considerably higher intensity of the β band and the occurrence of a prominent shoulder in that band originated from an additional electronic excitation. The mechanism of vibrational progressions associated with a single electronic excitation was further questioned by different polarizations of electronic transitions and analyses of excitation profiles in the resonance Raman (RR) spectrum.[27] Moreover, the oppositely signed features revealed in the CD and MCD spectra of MeCbl exposed the presence of two distinct electronic excitations in the α/β band region. To reconcile the differences between the original assignments[22] and their own spectroscopic data, Brunold and coworkers[27] concluded that vibrational progression associated with two different electronic transitions was required to explain the lowest-energy α/β band of MeCbl.

While the analysis of the Abs, CD, and MCD spectra has brought considerable advancement in understanding the electronic structure of vitamin B_{12} derivatives, the experimental and computational results summarized above must also be reconciled with other types of studies targeting the photochemical and photophysical properties of cobalamins, particularly those carried out by Sension and coworkers.[42–51] As demonstrated by Sension et al., useful information about the low-lying excited electronic states of B_{12} derivatives can be obtained with the aid of transient absorption spectroscopy (TAS). The TAS measurements by Sension et al. have indicated a diverse sensitivity of cobalamins to the excitation wavelength depending on the upper axial ligand. In the case of MeCbl considered in this work, an examination of the nature of metastable photoproduct has revealed a metal-to-ligand charge transfer (MLCT) character of the S_1 state, that is, a $d\rightarrow\pi^*$ transition.[42,44,46,50] Such an assignment is in clear contrast with the earlier proposals implying the $\pi\rightarrow\pi^*$ character of the $S_0\rightarrow S_1$ transition.

Although TD-DFT calculations using the hybrid B3LYP functional[39,40] tend to support a $\pi\rightarrow\pi^*$ assignment of the lowest-energy spectral band, there has been growing skepticism regarding the applicability of hybrid functionals for studying the electronic properties of B_{12} cofactors.[52–55] For this reason, the electronically excited states of B_{12} cofactors[56–59] have also been investigated using generalized-gradient-approximation-type (GGA-type) functionals, such as BP86.[60,61] It has been deduced that if one is interested in a larger number of MeCbl excited states, the utilization of at least two functionals (i.e., B3LYP and BP86) was required.[56] No single functional was capable of providing a uniformly accurate description of the entire electronic spectrum. However, the photochemistry of B_{12} cofactors, which is governed by the lowest-energy transitions only, was more appropriately described by BP86.[58,59] The BP86 functional has been shown to perform better than B3LYP in modeling axial bond properties[53,62] and has turned out to be more adequate in predicting the electronic excitations involving *d* orbitals of the cobalt metal. The studies reported in Ref. [56] have also identified the $S_0\rightarrow S_1$ excitation in MeCbl as a predominantly $\pi\rightarrow\pi^*$ transition when the B3LYP functional was applied in TD-DFT calculations, although some $d\rightarrow\pi^*$ contribution was also present due to the slight contribution of the d_{z^2} orbital in the HOMO participating in this transition. In contrast, the TD-DFT/BP86 results[58,59] have revealed a large amount of electron density originating from the Co d contributions to the HOMO and HOMO-1 that were associated with the first electronic transition in MeCbl, implying that the S_1 state of MeCbl should be characterized as an MLCT ($d/\pi\rightarrow\pi^*$) transition. Thus, the TD-DFT/B3LYP calculations were in line with the traditional $\pi\rightarrow\pi^*$ interpretation of the $S_0\rightarrow S_1$ band, whereas the TD-DFT/BP86 implied an MLCT transition, consistently with the analysis of TAS data.[42,44,46,50]

The significant step toward understanding the nature of excited states in B_{12} derivatives has been achieved when, in addition to the Abs data, the CD and MCD spectra of CNCbl and MeCbl were computed and compared with experiment.[63] Two different functionals, namely, CAM-B3LYP and BP86, were applied to simulate the electronic spectra of CNCbl and MeCbl, and it has been concluded that better agreement with experiment was provided by the BP86 functional. It has also been noticed, however, that the Abs data alone were not sufficient to justify the use of one functional over another. Moreover, it has been determined that multiple electronic transitions contribute to the α/β band observed for both cobalamins.[63]

The above discussion demonstrates that the nature of the S_1 state of MeCbl cofactor remains elusive, since the existing experimental and theoretical predictions do not yield a consistent picture regarding its electronic structure. Clearly, a proper description of the energetically lowest excited state of MeCbl requires additional independent analyses, particularly those based on higher level *ab initio* wavefunction-based methodologies. The purpose of the present contribution is to provide such new insights. Two different higher level *ab initio* methods are used to determine the low-lying states of MeCbl, namely, the modified version of the second-order multiconfigurational quasi-degenerate perturbation theory (MC-QDPT2),[64] (abbreviated as MC-XQDPT2, using complete active space self-consistent field (CASSCF)[65] reference wave functions, which has previously been applied in the study of CNCbl),[66] and the single-reference equation-of-motion coupled-cluster singles and doubles (EOM-CCSD) approach,[67,68] which has never been used before to examine the cobalamin spectra, but is known to provide a reasonable description of excited states dominated by one-electron transitions, including charge-transfer (CT) excitations. Taking into account the strong dependence of the TD-DFT results on the applied functional, a number of TD-DFT calculations have been performed and benchmarked against the MC-XQDPT2 and EOM-CCSD *ab initio* data. In addition to B3LYP[39,40] and BP86,[60,61] a few other functionals, including hybrid (MPW1PW91,[69,70] TPSSh[71]), GGA-type (BLYP,[40,72] MPWPW91[70,73]), meta-GGA (TPSS[74]), and range-separated (CAM-B3LYP[75] and LC-BLYP[76]) approaches, have been used in the present computations. The latter two functionals were used to address the potential problem caused by underestimation of the TD-DFT excitation energies having a significant CT character.[77–79] In particular, the effect of varying the Hartree–Fock (HF) exchange and correlation contributions in the exchange-correlation functional was investigated by computing the excited-state properties of MeCbl as a function of the range-separation parameter μ.

Computational Details

Structural models

To reduce computational costs, the majority of the previous theoretical studies of the B_{12} cofactors used simplified models with respect to side chains. Such an approach demonstrated satisfactory results in predicting their structural and electronic properties.[27–29,36–38,52–59,62,80] Consequently, a truncated structure of the MeCbl cofactor, that is, the Im-[Co^{III}(corrin)]-CH_3^+ model having 58 atoms shown in Figure 2, was exploited in

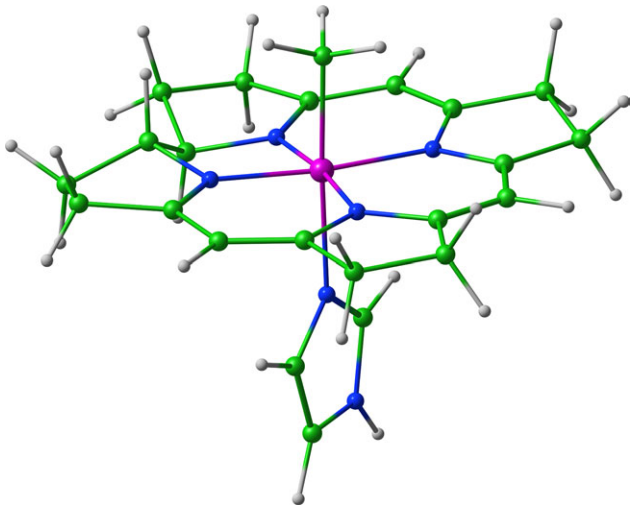

Figure 2. Structural model of MeCbl, abbreviated as Im-[Co^{III}(corrin)]-CH_3^+, used in the present study. [Color figure can be viewed in the online issue, which is available at wileyonlinelibrary.com.]

the present study. Using the X-ray crystallographic data for the full MeCbl structure[81] as a starting point for designing the Im-[Co^{III}(corrin)]-CH_3^+ model, we replaced all amide side chains of the corrin ring with the hydrogen atoms while truncating the nucleotide loop at C_{17}, leaving the resulting structure positively charged. Under enzymatic conditions, in B_{12}-dependent methyltransferases,[6,9,16,18] the dimethylbenzimidazole (DBI) base is replaced by the histidine (His) residue from the protein side chain. Thus, the lower axial DBI fragment was substituted by imidazole (Im). The final Im-[Co^{III}(corrin)]-CH_3^+ structure was optimized at the BP86/6-31G(d) level (using spherical d functions). The corresponding Cartesian coordinates can be found in the Supporting Information. As shown in Ref. [55], the optimized structural parameters of the Im-[Co^{III}(corrin)]-CH_3^+ system are almost insensitive to the functional used, and the structure of Im-[Co^{III}(corrin)]-CH_3^+ obtained in the BP86/6-31G(d) calculations is in good agreement with the X-ray data for *Coα*-(1*H*-Imidazolyl)-Co*β*-methylcob(III)amide.[82]

CASSCF/MC-XQDPT2 calculations

To examine the properties of the low-lying excited states of MeCbl, as modeled by the Im-[Co^{III}(corrin)]-CH_3^+ system shown in Figure 2, both CASSCF- and MC-XQDPT2-level calculations were carried out. The latter calculations, aimed at correcting the CASSCF excitation energies for the leading dynamical correlation effects, were performed using the modified version of the MC-QDPT2 approach of Ref. [64], abbreviated as MC-XQDPT2, as implemented in the PCGAMESS/Firefly quantum chemistry package.[83] We recall that the MC-XQDPT2 approach is a genuine multiroot (i.e., perturb-then-diagonalize) multireference perturbation theory technique using the CASSCF state-averaged (SA) electron density over the ground and excited states of interest, which allows a true mixing of the CASSCF zero-order states via the construction and the subsequent diagonalization of the effective Hamiltonian. Typically, to obtain accurate results, the excited-state, CASSCF-based, MC-XQDPT2 calculations require a determination of a manifold of electronic states for the proper analysis of the low-lying excited states of interest, particularly for transition-metal systems, such as cobalamins,[66] where there may be several low-lying electronic states that interact one with another. As a result, 20 electronic states were considered in the SA-CASSCF calculations preceding the final MC-XQDPT2 work to investigate the nature of the four lowest-energy excited states at the MC-XQDPT2 level of theory. The CASSCF/MC-XQDPT2 calculations were performed using the 6-31G(d) basis with spherical d orbitals, assuming the BP86/6-31G(d) optimized geometry of the Im-[Co^{III}(corrin)]-CH_3^+ system. The details of the active orbital space used in the CASSCF/MC-XQDPT2 calculations reported in this work are discussed in Section 3.2. The 38 lowest-energy core orbitals that correlate with the 1s shells of the carbon and nitrogen atoms, and the 1s, 2s, 2p, 3s, and 3p shells of Co were frozen in the MC-XQDPT2 calculations.

EOM-CCSD calculations

The EOM-CC-type calculations were carried out at the basic EOM-CCSD[67,68] or the equivalent linear response CCSD level,[84,85] which is considered to be appropriate if the excited states of interest are dominated by one-electron transitions,[86–88] as is the case in this study, where the low-lying states of the Im-[Co^{III}(corrin)]-CH_3^+ model of MeCbl are examined. The EOM-CCSD approximation provides reasonable results for such states, with errors in the excitation energies on the order of 0.1 eV in calculations for smaller systems[67,68,84–88] and typically in the 0.3–0.5 eV range for larger polyatomic molecules (see Refs. [89–93] for examples).

Let us recall that in the EOM-CCSD method, one represents excited electronic states $|\Psi_\mu\rangle$ by applying the linear excitation operator $R_\mu^{(CCSD)} = R_{\mu,0} + R_{\mu,1} + R_{\mu,2}$ ($R_{\mu,n}$ is the *n*-body or *n*-tuply excited component of $R_\mu^{(CCSD)}$) to the ground state $|\Psi_0\rangle = e^{T_1+T_2}|\Phi\rangle$ resulting from the standard CCSD[94–97] calculations. Here, T_1 and T_2 are the singly and doubly excited components of the cluster operator $T^{(CCSD)} = T_1 + T_2$ obtained in the ground-state CCSD calculations and $|\Phi\rangle$ is the reference determinant. Note that we used the restricted HF (RHF) determinant as a reference in our calculations. The EOM-CCSD excitation operators $R_\mu^{(CCSD)}$ and the corresponding vertical excitation energies $\omega_\mu^{(CCSD)} = E_\mu^{(CCSD)} - E_0^{(CCSD)}$ are obtained by diagonalizing the similarity-transformed Hamiltonian $\overline{H}^{(CCSD)} = e^{-T^{(CCSD)}}He^{T^{(CCSD)}}$ resulting from the CCSD calculations in a space of singly and doubly excited determinants relative to $|\Phi\rangle$.

The EOM-CCSD calculations reported in the present study and the corresponding ground-state CCSD calculations were

performed using the CC and EOM-CC computer programs described in Refs. [98] and [99] that are part of the GAMESS package.[100,101] In analogy to the MC-XQDPT2 case, the 38 lowest-energy core orbitals that correlate with the 1s shells of the carbon and nitrogen atoms, and the 1s, 2s, 2p, 3s, and 3p shells of cobalt were frozen in the CCSD and subsequent EOM-CCSD iterations. As in the case of the CASSCF/MC-XQDPT2 computations and due to the enormous computer costs of the CCSD and EOM-CCSD calculations for molecular systems of the Im-[Co^{III}(corrin)]-CH_3^+ size, where we had to correlate 158 electrons outside the frozen core, the 6-31G(d) basis set was used (using spherical components of the d functions). Again, the ground-state nuclear geometry of Im-[Co^{III}(corrin)]-CH_3^+ used in the EOM-CCSD calculations of vertical excitation energies for this system was obtained from the aforementioned BP86/6-31G(d) optimization. We attempted to determine four excited states, but we could not converge the fourth one, so the EOM-CCSD results presented in this work are limited to the $S_0 \rightarrow S_n$ excitations with $n = 1$, 2, and 3.

TD-DFT calculations with different functionals

The low-lying excited states of MeCbl, as modeled by the Im-[Co^{III}(corrin)]-CH_3^+ structure, were also calculated using a variety of TD-DFT approaches. Nine different functionals were used to examine the performance of TD-DFT against the high-level MC-XQDPT2 and EOM-CCSD data. In addition to the standard B3LYP and BP86 choices, seven other functionals, including BLYP, TPSSh, TPSS, MPW1PW91, MPWPW91, CAM-B3LYP, and LC-BLYP, were used. Since the recent studies of MeCbl, examining the performance of different functionals in predicting the Co—C_{Me} bond dissociation energy, indicated that the GGA-type functionals were capable of producing results that were quite close to the experimental and high-level *ab initio* dissociation energies,[55] three such functionals, namely, BLYP, MPWPW91, and TPSS, were tested and compared with their hybrid B3LYP, MPW1PW91, and TPSSh analogs, having different fractions of the exact HF exchange (20, 25, and 10%, respectively). The Coulomb-attenuating CAM-B3LYP[75] method and range-separated LC-BLYP approach[69,77–79] were used to address the possible underestimation of the TD-DFT excitation energies for CT transitions. The LC-BLYP approach allows for an effective tuning of the relative contributions to the exchange-correlation potential originating from the exchange and correlation terms via the range separation parameter, μ. Thus, the LC-BLYP vertical excitation energies were calculated as a function of μ ranging from 0 to 0.90 $Bohr^{-1}$, with an increment of 0.10 $Bohr^{-1}$.

The TD-DFT calculations of the low-lying excited states of Im-[Co^{III}(corrin)]-CH_3^+ were carried out using the 6-31G(d) basis set using the spherical d orbitals. The basis set dependence of the resulting excitation energies was examined by performing TD-DFT calculations with a larger 6-311++G(d,p) basis. As shown below, the use of a larger basis set has essentially a negligible effect on the key characteristics of the low-lying states, particularly on the S_1 state, which is the main subject of the present work.

To verify the influence of the ground-state geometry on the TD-DFT vertical excitations energies, two different approaches were explored, namely, (i) the TD-DFT calculations using different functionals, but using the same, BP86/6-31G(d) optimized ground-state structure of the Im-[Co^{III}(corrin)]-CH_3^+ model and (ii) the TD-DFT calculations using the ground-state geometries of Im-[Co^{III}(corrin)]-CH_3^+ optimized with the same functional as applied in the excited-state calculations. For each functional explored in this study, the excitation energies obtained using the above two approaches turned out to be practically identical. For this reason, in our discussion below, we focus on the results obtained with the second approach. The exceptions are the LC-BLYP vertical excitation energies, which are based on the BP86/6-31G(d) optimized structure. The TD-DFT calculations using the B3LYP, BP86, BLYP, TPSSh, TPSS, MPW1PW91, MPWPW91, and CAM-B3LYP functionals were performed using the Gaussian 09 suite of programs.[102] The LC-BLYP calculations using different values of μ were carried out using a locally modified version of the GAMESS software.[100,101] Finally, the TD-DFT/BP86 geometry optimization of the S_1 state was performed with TURBOMOLE.[103]

Results and Discussion

Experimental information about the low-lying excited states of MeCbl

The analysis of the low-lying excited states of MeCbl cofactor has been the subject of several experimental investigations. The most recent results originate from the TAS studies by Sension et al.[42,44,46,50] and the spectroscopic studies by Brunold and coworkers.[27,30] Since the latter group analyzed the details of the Abs as well as the CD and MCD spectra, our computed excitations are compared with the results obtained by Brunold et al.

According to the analysis of Abs, CD, and MCD data reported by Brunold and coworkers,[27] at least four bands contribute to the Abs envelope in the α/β spectral range. The excitation energies, which correspond to the maxima of the four Gaussian bands found by Brunold et al. using the iterative fitting of the Abs, CD, and MCD spectra, are 2.22 eV (band 1), 2.35 eV (band 2), 2.55 eV (band 3), and 2.70 eV (band 4) (see Table 1 and footnote b in it). The splitting between bands 2 and 3, of about 0.20 eV, is larger than that between bands 1 and 2 ($\sim$0.13 eV), implying that the four bands identified by Brunold et al. do not represent vibrational progressions associated with a single electronic transition. Furthermore, a detailed analysis of the CD and MCD data shows that bands 1 and 2 have opposite signs in comparison with bands 3 and 4. Based on all of this information, Brunold and coworkers arrived at the conclusion that one should associate two distinct electronic transitions with the α/β spectral range, which are characterized by the 0-0 excitation energies of 2.22 and 2.55 eV and that the lowest one should be interpreted as a $\pi \rightarrow \pi^*$ excitation of corrin.[27] According to this interpretation, the remaining two bands that result from the Gaussian deconvolution of the α/β spectral region carried out in Ref. [27], with the

Table 1. Vertical excitation energies (eV) of the lowest four excited states of Im-[Co^{III}(corrin)]-CH_3^+ calculated with different methods and the 6–31G(d) basis set.

Method	S_1	S_2	S_3	S_4
Ab initio				
CASSCF(12,12)	3.21	3.34	4.47	4.60
MC-XQDPT2	2.48	2.67	2.79	3.42
EOM-CCSD	2.65	3.12	3.23	[a]
TD-DFT				
B3LYP (20% HF)	2.65	2.82	2.95	3.02
CAM-B3LYP	2.87	2.92	3.00	3.06
BLYP	2.19	2.33	2.48	2.58
LC-BLYP ($\mu = 0.00$)	2.20	2.35	2.48	2.62
LC-BLYP ($\mu = 0.10$)	2.27	2.44	2.53	2.67
MPW1PW91 (25% HF)	2.70	2.85	2.96	3.02
MPWPW91	2.19	2.35	2.48	2.58
TPSSh (10% HF)	2.52	2.79	2.85	3.14
TPSS	2.29	2.44	2.55	2.75
BP86	2.18	2.34	2.48	2.59
Experiment[b]				
Abs, CD, and MCD	2.22	2.35[c]	2.55	2.70[d]

[a] The fourth EOM-CCSD root did not converge. [b] The results obtained in Ref. [27] using the Gaussian deconvolution of the Abs spectrum in the α/β range, which gives four bands with maxima at 17,870, 18,950, 20,550, and 21,800 cm^{-1}. [c] Interpreted in Ref. [27] as a vibrational progression of the transition at 2.22 eV. [d] Interpreted in Ref. [27] as a vibrational progression of the transition at 2.55 eV.

maxima at 2.35 and 2.70 eV, belong to the overlapping vibrational progressions associated with the two electronic transitions that have the 0-0 excitation energies of 2.22 and 2.55 eV, respectively. Although this certainly is a plausible explanation, there are potential issues with it, some acknowledged by the authors of Ref. [27], that consequently leaves room for alternative interpretations. First of all, one has to consider the above interpretation with caution, since the analysis of the Abs, CD, and MCD data reported in Ref. [27] is based on the Gaussian deconvolution technique. Gaussian deconvolution is an iterative fitting procedure which assumes the smallest possible number of Gaussian bands to resolve the major electronic transitions contributing to the particular spectral window and does not guarantee that certain low-intensity electronic transitions are not omitted from the fitting procedure. In other words, one cannot exclude the scenario that the number of electronically excited states of MeCbl that contribute to the α/β spectral region is greater than that predicted by the Gaussian deconvolution exploited in Ref. [27]. Another issue related to the interpretation of the α/β spectral region, as originating from the $\pi\rightarrow\pi^*$ electronic transition accompanied by the corresponding vibrational progressions, is the intensity ratio. Typically, one observes intensity lowering when the second member of the vibrational progression is compared with the 0-0 transition. However, in the MeCbl case, the opposite pattern is observed; that is, the second band centered at 2.35 eV has a larger intensity than the first one at 2.22 eV. The next potential problem with the interpretation of the α/β spectral region, as originating from only the $\pi\rightarrow\pi^*$ electronic transition, is related to the strong enhancement of the Co—C_{Me} stretching mode, which resembles an isolated harmonic oscillator perpendicular to the corrin plane. If the S_1 state was a $\pi\rightarrow\pi^*$ transition, an in-plane mode would be strongly enhanced in the RR spectrum when the laser excitation was tuned to this particular spectral region. This, however, contradicts the available RR data acquired for the resonance with the longer-wavelength absorption band at 530.9 nm, where strong enhancement of the Co—C_{Me} stretch at 506 cm^{-1} is observed.[104] The RR experiments also suggest that the π system of corrin should be electronically coupled to the Co—C_{Me} bond to weaken it with the electronic excitation. It is, in principle, possible that one of the higher excited states S_n with $n > 1$, with a noticeable transition dipole, provides such a coupling. This, however, seems rather unlikely, since, at least according to TD-DFT calculations with hybrid functionals,[27] the states of interest are energetically higher and may, in fact, lie outside of the α/β spectral range. It is true that such a coupling could also be provided by the S_1 state, as implied by the findings in Ref. [27], but this would then contradict the interpretation of the $S_0\rightarrow S_1$ transition as a $\pi\rightarrow\pi^*$ excitation in corrin. All of this suggests that the $\pi\rightarrow\pi^*$ character of the low-lying excited states of MeCbl, particularly S_1, can be questioned and that the alternative MLCT interpretation of the S_1 state, postulated by Sension et al.,[42,44,46,50] is possible as well.

Electronic excitations resulting from the CASSCF/MC-XQDPT2 calculations

Ab initio methods based on the CASSCF methodology are frequently regarded as useful tools for studying electronically excited states.[105–108] However, when performing CASSCF and other CASSCF-based multireference computations, such as those based on the MC-XQDPT2 approach, one has to select active orbitals in a judicious manner, particularly in the case of larger molecules containing transition metals and tetrapyrrolic ligands, such as corrin. The number of active orbitals that may have to be considered in these systems can easily become very large, making the CASSCF-based calculations prohibitively expensive or even technically impossible. At the same time, the results of CASSCF-based calculations may strongly depend on the choice of the active space. It is, therefore, important to find a proper balance between chemical intuition used to identify meaningful active orbitals relevant to the problem of interest and the size of the resulting active space that has to be computationally manageable.

In the case of the CASSCF and CASSCF-based MC-XQDPT2 calculations for the Im-[Co^{III}(corrin)]-CH_3^+ model of MeCbl, reported in this work, the process of selecting active orbitals was guided by the active spaces that were previously used for the various derivatives of cobalt corrinoids.[66,109–112] Let us recall that although the MeCbl cofactor belongs to cobalamins, a class of Co^{III} octahedral complexes, the local environment of cobalt in Im-[Co^{III}(corrin)]-CH_3^+ causes the splitting of the d orbitals consistent with the square-planar structure, which has a d^6 configuration as the dominant electronic configuration. According to crystal field theory, such an electronic configuration leaves the highest $d_{x^2-y^2}$ orbital empty, that is, in designing meaningful active spaces for the CASSCF and CASSCF-

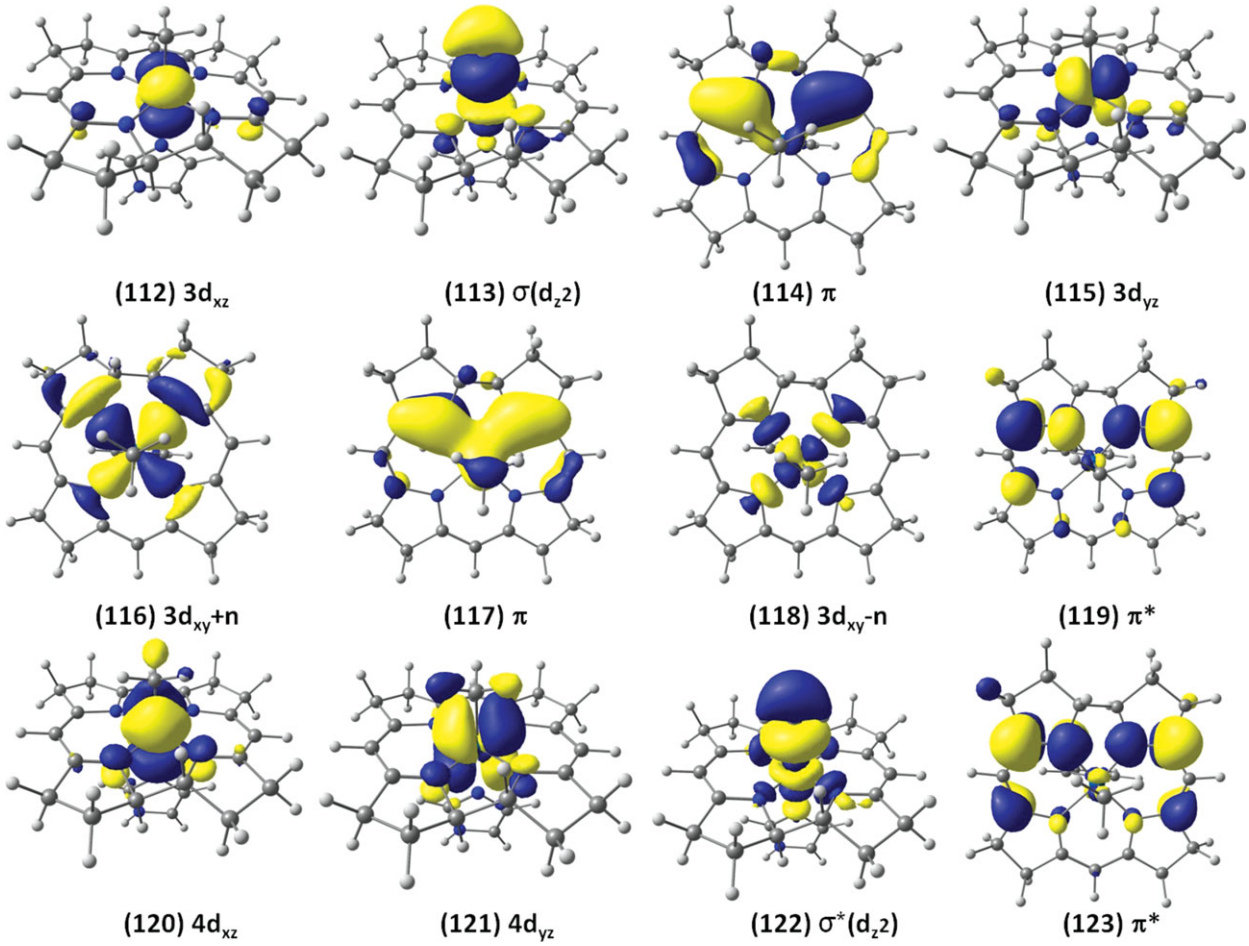

Figure 3. Active orbitals of Im-[Co^{III}(corrin)]-CH_3^+ used in the CASSCF(12,12) and subsequent MC-XQDPT2(12,12) calculations. [Color figure can be viewed in the online issue, which is available at wileyonlinelibrary.com.]

based MC-XQDPT2 calculations for the Im-[Co^{III}(corrin)]-CH_3^+ system, one may focus on the d_{xy}, d_{xz}, d_{yz}, and d_{z^2} orbitals of Co, mixed up with the appropriate orbitals of the corrin and methyl fragments. Here and elsewhere in this description, in labeling the d orbitals of Co, we are assuming that the *z*-axis is perpendicular to the corrin macrocycle. Furthermore, the *x* and *y* axes that define the *xy*-plane of the corrin backbone are oriented such that the C_2 axis of symmetry coincides with the *x*-axis. This choice of the coordinate system corresponds to a 45° rotation of the *x* and *y* axes compared to the previous study of cob(I)alamin by Jensen.[109] Keeping in mind the above coordinate frame and adding the 4d correlating orbitals to the doubly occupied 3d orbitals to account for the double shell effect in transition metal complexes,[108] we ended up with the following four subgroups of orbitals in our final active space design (see Fig. 3): (i) the doubly occupied $3d_{xz}$ and $3d_{yz}$ orbitals centered on the Co atom and the corresponding correlating orbitals of the 4d type, that is, $4d_{xz}$ and $4d_{yz}$, (ii) the bonding Co—C_{Me} $\sigma(d_{z^2})$ orbital and its antibonding $\sigma^*(d_{z^2})$ counterpart, (iii) the occupied $3d_{xy}$ + n and unoccupied $3d_{xy}$ − n orbitals describing the respective bonding and antibonding combinations of the $3d_{xy}$ orbital centered on the Co atom with the lone pairs (n) centered on the four equatorial nitrogens in the corrin plane, and (iv) the two occupied π and two unoccupied π^* orbitals of corrin. While the inclusion of active orbitals that belong to the (ii) and (iii) subgroups was mandatory for a proper description of the equatorial and axial σ-interactions, leaving no room for maneuver, the selection of active orbitals that has ultimately resulted in subgroups (i) and (iv) turned out to be less straightforward. Therefore, we had to come up with an active space which was chemically meaningful and, at the same time, did not have more than a dozen orbitals to make the resulting CASSCF and MC-XQDPT2 calculations computationally feasible. Thus, in the initial stages of our work, several active orbital spaces were tested, mostly by selecting different subsets of orbitals that correlate with the 3d and 4d shells of Co and π network of corrin. Additional analyses were carried out to eliminate those molecular orbitals (MOs) that did not significantly contribute to the CASSCF wave functions relevant to the electronic states of interest (as measured, e.g., by the occupation numbers of the natural orbitals of CASSCF). As a result, the final active space used in the CASSCF and MC-XQDPT2 calculations for Im-[Co^{III}(corrin)]-CH_3^+ reported in this work consisted of 12 active electrons distributed among 12 active orbitals, which corresponded to the above subgroups (i)–(iv). Four occupied d-type orbitals of Co and two occupied π-type orbitals localized on corrin were combined with the six corresponding virtual orbitals to obtain

Table 2. The ground and four lowest excited states of Im-[Co^{III}(corrin)]-CH_3^+ obtained from the CASSCF-based MC-XQDPT2 calculations. CSF stands for a configuration state function.

State	E(eV)	f	Weight (%) of CAS state in MC-XQDPT2	CAS state	Coefficient of CSF (%)	Character
S_0	0		88	1		
S_1	2.48	0.0022	52	12	22	$d_{xz} \rightarrow \pi^*$
			16	10	24	$d_{yz}/\pi \rightarrow d_{xy} + \sigma^*/\pi^*$
					18	$d_{xz}/\pi \rightarrow d_{xy} + \sigma^*/\pi^*$
S_2	2.67	0.0452	45	14	12	$d_{yz} \rightarrow \pi^*$
					30	$d_{xz} \rightarrow \pi^*$
			27	11	36	$d_{yz} \rightarrow \pi^*$
					4	$\pi \rightarrow \pi^*$
					11	$d_{xz} \rightarrow \pi^*$
			19	13	26	$d_{yz} \rightarrow \pi^*$
					4	$\pi \rightarrow \pi^*$
					9	$d_{xz} \rightarrow \pi^*$
S_3	2.79	0.2536	39	11	36	$d_{yz} \rightarrow \pi^*$
					4	$\pi \rightarrow \pi^*$
					11	$d_{xz} \rightarrow \pi^*$
			23	13	26	$d_{yz} \rightarrow \pi^*$
					4	$\pi \rightarrow \pi^*$
					9	$d_{xz} \rightarrow \pi^*$
			20	12	22	$d_{xz} \rightarrow \pi^*$
S_4	3.42	0.0421	32	14	12	$d_{yz} \rightarrow \pi^*$
					30	$d_{xz} \rightarrow \pi^*$
			30	13	26	$d_{yz} \rightarrow \pi^*$
					4	$\pi \rightarrow \pi^*$
					9	$d_{xz} \rightarrow \pi^*$

the optimal set of active MOs (Fig. 3) for elucidating the nature of the S_1 state.

As shown in Table 1, the vertical excitation energies obtained in our CASSCF(12,12) calculations are considerably higher than those observed experimentally. For example, the energy of the lowest excited S_1 state is almost 1 eV higher than the corresponding experimental energy. The CASSCF results obtained here for the Im-[Co^{III}(corrin)]-CH_3^+ model of MeCbl are similar to those characterizing the CNCbl derivative, where the analogous overestimation of the excitation energies was observed and subsequently improved by including dynamical correlation effects via the MC-XQDPT2 theory. In addition, the inspection of the lowest-energy excited states of MeCbl predicted by CASSCF reveals that they are dominated by d→d transitions (see Supporting Information Table S1), which is a problematic finding. Such a poor description of the low-lying electronic states reflects a downside of using the CASSCF method alone, as previously argued in the case of CNCbl.[66] One has to calculate many more excited states at the CASSCF level, enable their intrinsic mixing at the correlated theory level to improve the zero-order description, and include dynamical correlation effects on top of CASSCF to obtain a more quantitative description. This can be done through the use of the multireference, multiroot (i.e., perturb-then-diagonalize), perturbation theory, represented in this study by the MC-XQDPT2 approach.

As shown in Tables 1 and 2, the inclusion of dynamical correlation effects via the MC-XQDPT2 methodology dramatically improves the excitation energies characterizing the Im-[Co^{III}(corrin)]-CH_3^+ system. Indeed, the MC-XQDPT2 approach reduces the CASSCF vertical excitation energies corresponding to the $S_0 \rightarrow S_1$, $S_0 \rightarrow S_2$, $S_0 \rightarrow S_3$, and $S_0 \rightarrow S_4$ transitions, of 3.21, 3.34, 4.47, and 4.60 eV, by 0.73, 0.67, 1.68, and 1.18 eV, respectively, bringing at least three of them to a reasonably good agreement with the excitation energies observed experimentally. In particular, the MC-XQDPT2 result for the S_1 state, which is the main focus of this work, differs from the corresponding experimental excitation energy by only 0.26 eV, which is an excellent description. We note, however, that these considerable improvements would not be possible if we did not calculate many additional CASSCF states and if we did not allow their intrinsic mixing at the multireference perturbation theory level. As shown in Figure 4, the electronic states of the

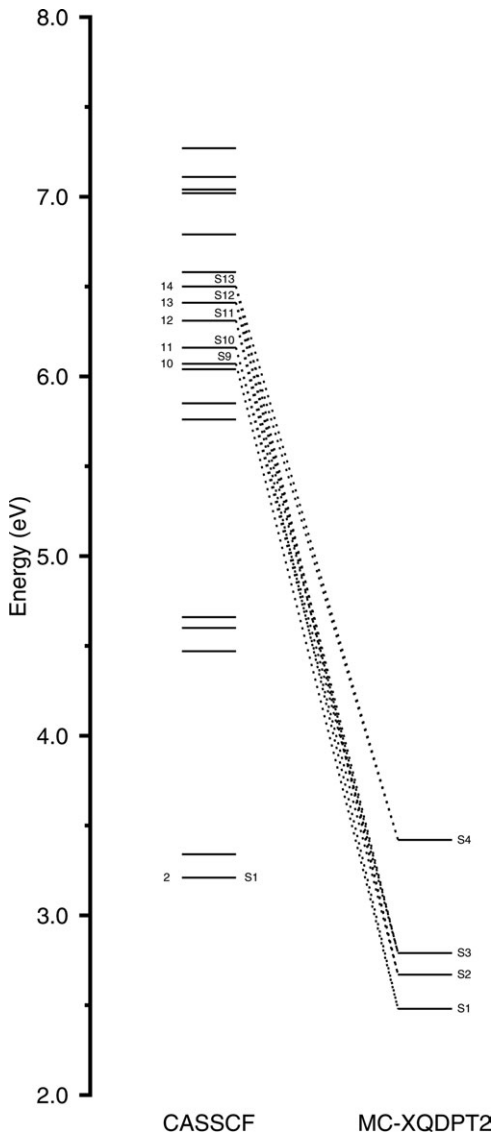

Figure 4. The lowest 20 excited states computed at the CASSCF(12,12) level and the four lowest-energy excited states resulting from the corresponding MC-XQDPT2 calculations. The lines between the CASSCF and MC-XQDPT2 energy levels indicate mixing of states upon the incorporation of dynamical correlation effects via the second-order perturbation theory (see Table 2 for further details).

Table 3. The lowest three excited states of Im-[Co^{III}(corrin)]-CH$_3^+$ obtained from EOM-CCSD calculations.

State	E (eV)	Amplitudes[a]		Character	
S_1	2.65	R1	−0.0912	114 → 118	$\sigma(d_{z^2}/d_{x^2-y^2})/\pi \rightarrow \pi^*$
		R1	−0.6232	117 → 118	$\pi/\sigma(d_{z^2}) \rightarrow \pi^*$
		R1	−0.1506	116 → 119	$\pi \rightarrow \pi^*$
		R1	0.0595	113 → 120	$\pi/\sigma(d_{z^2}/d_{xz}) \rightarrow \pi^*$
		R2	−0.0552	117,116 → 118,118	$\pi/\sigma(d_{z^2}), \pi \rightarrow \pi^*$
		R2	−0.0552	116,117 → 118,118	$\pi, \pi/\sigma(d_{z^2}) \rightarrow \pi^*$
S_2	3.12	R1	0.3076	80 → 139	$d_{x^2-y^2}/\sigma_{Corr}/\sigma_{Im} \rightarrow d_{xy} + n$
		R1	−0.1683	95 → 139	$\sigma_{Corr}/d_{x^2-y^2} \rightarrow d_{xy} + n$
		R1	−0.1494	79 → 139	$d_{yz}/\sigma_{Im} \rightarrow d_{xy} + n$
		R1	0.1383	80 → 131	$d_{x^2-y^2}/\sigma_{Corr}/\sigma_{Im} \rightarrow \sigma_{Corr}^*$
		R1	−0.1363	75 → 139	$\sigma_{Corr}/d_{x^2-y^2} \rightarrow d_{xy} + n$
		R1	−0.1320	85 → 139	$\sigma_{Corr}/d_{x^2-y^2} \rightarrow d_{xy} + n$
		R1	0.1018	81 → 139	$\sigma_{Im}/d_{yz} \rightarrow d_{xy} + n$
S_3	3.23	R1	0.1494	81 → 139	$\sigma_{Im}/d_{yz} \rightarrow d_{xy} + n$
		R1	0.1335	80 → 139	$d_{x^2-y^2}/\sigma_{Corr}/\sigma_{Im} \rightarrow d_{xy} + n$
		R1	−0.1220	75 → 139	$\sigma_{Corr}/d_{x^2-y^2} \rightarrow d_{xy}+n$
		R1	0.1103	81 → 132	$\sigma_{Im}/d_{yz} \rightarrow \pi^*/\sigma(d_{z^2})$
		R1	0.1090	78 → 139	$d_{xz}/\sigma_{Im} \rightarrow d_{xy} + n$

[a] For the S_2 and S_3 states, only the transitions with excitation amplitudes R greater than 0.1000 are presented. See Supporting Information (Table S15) for a more complete list.

Im-[Co^{III}(corrin)]-CH$_3^+$ system undergo a significant reordering when the dynamical correlation effects are turned on via the MC-XQDPT2 theory. In particular, the CASSCF states that contribute to the four lowest-energy excited states of Im-[Co^{III}(corrin)]-CH$_3^+$ in the MC-XQDPT2 description most significantly can be identified as roots 10–14 (or S_9–S_{13}) in the CASSCF spectrum (see Fig. 4 and Table 2). This has several interesting consequences. One of the most important consequences is the observation that the physical nature of the computed excited states alters when the reordering and mixing of the CASSCF states is allowed and when the dynamical correlation effects are turned on. As shown in Table 2, the four lowest-energy excited states of Im-[Co^{III}(corrin)]-CH$_3^+$ calculated at the MC-XQDPT2 level have substantial components from single d→π^* and double d/π→π^* transitions. In particular, the MC-XQDPT2 wave function of the S_1 state, which interests us here the most, is primarily composed of the 10th (16 %) and 12th (52%) states from the CASSCF spectrum. The main contribution to the latter CASSCF wave function, which dominates the MC-XQDPT2 S_1 state, is a d→π^* transition, whereas the former CASSCF state has a predominantly d/π→d + σ/π^* character (see Table 2). In other words, the lowest-energy excited state of the Im-[Co^{III}(corrin)]-CH$_3^+$ system in the MC-XQDPT2 description can be characterized as an MLCT d→π^* transition that originates from large d→π^* CT excitations defining the 12th root in the underlying CASSCF spectrum. As shown in Table 2, both the S_2 and S_3 states include substantial contributions from the 11th CASSCF state, which has a d_{yz}/d_{xz}→π^* character, and the S_2 state has also very large (in fact, dominant) contributions from the 14th CASSCF state, which is mainly composed of d_{xz}→π^* and d_{yz}→π^* transitions. Thus, the three lowest-energy excited states of the Im-[Co^{III}(corrin)]-CH$_3^+$ system resulting from the MC-XQDPT2 computations, which fall within 0.2–0.3 eV from the bands observed experimentally in the α/β region, can be interpreted as MLCT d→π^* transitions. The same applies to the S_4 state (see Table 2). According to our MC-XQDPT2 calculations, none of the lowest-energy excited states of Im-[Co^{III}corrin]-CH$_3^+$ can be described as π→π^* transitions localized on corrin; they all are of the d→π^* type, instead.

Electronic excitations resulting from the EOM-CCSD calculations

The low-lying excited states of the Im-[Co^{III}(corrin)]-CH$_3^+$ model of MeCbl were also examined using EOM-CCSD. The ground-state CCSD and excited-state EOM-CCSD calculations were carried out using a ground-state RHF determinant as a reference. Four excited states were requested, but we could not converge the fourth EOM-CCSD root. Consequently, only three lowest excited states of Im-[Co^{III}corrin]-CH$_3^+$ found in the EOM-CCSD calculations were taken into consideration for further analysis.

As mentioned earlier, the EOM-CCSD method is considered to be appropriate when the excited states of interest are dominated by one-electron (including CT) transitions. Careful inspection of the largest R_1 and R_2 amplitudes defining the EOM-CCSD wave functions of the S_1, S_2, and S_3 states reveals that dominant contributions to these states, indeed, originate from one-electron transitions (see Table 3 and Fig. 5). As pointed out in Section 2, for such states, particularly when large polyatomic molecules, such as Im-[Co^{III}(corrin)]-CH$_3^+$, are considered, one can anticipate that errors in the excitation energies resulting from the EOM-CCSD calculations are in the 0.3–0.5 eV range. As shown in Table 1, the first electronic excitation in the EOM-CCSD spectrum is 0.43 eV above the experimental S_0→S_1 transition, that is, it falls within the expected error range. However, larger differences, of 0.77 eV in the case of S_2 and 0.68 eV in the case of S_3, are observed when the EOM-CCSD results for these two states are compared with experiment. It is, therefore, unclear whether the S_2 and S_3 states found in our calculations significantly contribute to the observed α/β bands. The EOM-CCSD excitation energy characterizing the S_1 state is also in excellent agreement with that obtained in the MC-XQDPT2 calculations (a small, 0.17 eV, difference), but the energies of the S_2 and S_3 states are again rather different, with differences falling into the 0.4–0.5 eV range (see Table 1). One should re-emphasize though that such an overestimation of excitation energies in the EOM-CCSD calculations for larger molecular systems is not unusual and that the EOM-CCSD wave functions remain perfectly meaningful in spite of such energy differences as long as the electronically excited states of interest are dominated by one-electron transitions.[89–93] For example, the similarly overestimated excitation energies have been observed in the highly

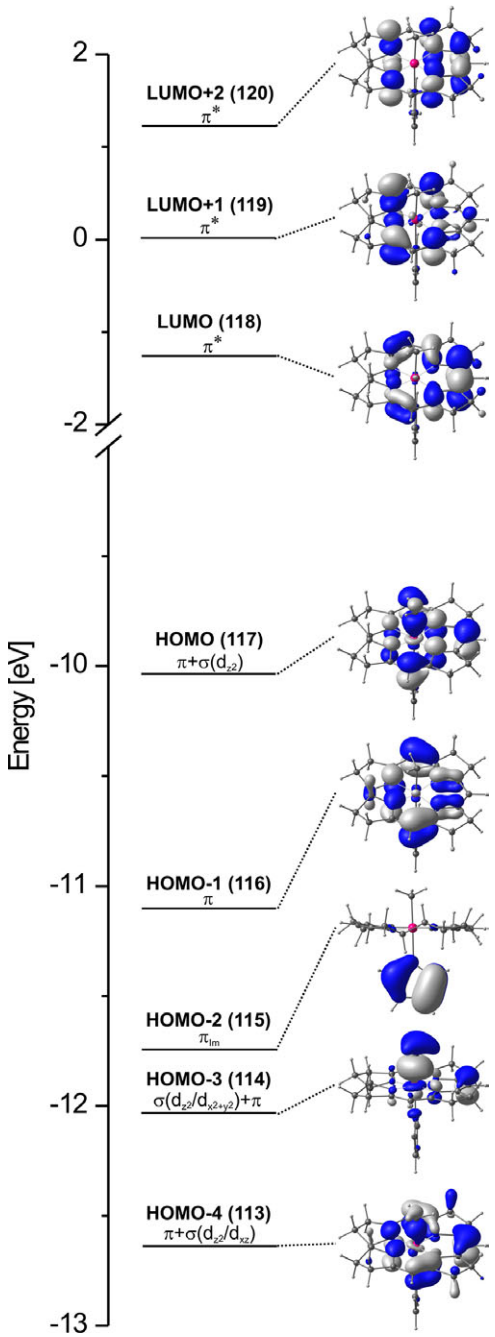

Figure 5. Canonical RHF orbitals used in the CCSD and EOM-CCSD calculations. [Color figure can be viewed in the online issue, which is available at wileyonlinelibrary.com.]

successful calculations of the electronic spectra of metalloporphyrins using the symmetry-adapted-cluster configuration-interaction[113–115] and linear-response coupled-cluster[84,85] methods with singles and doubles, which are closely related to the EOM-CCSD approach used in this work (see Refs. [116–118] for a few representative examples).

The nature of the lowest excited states of MeCbl resulting from the EOM-CCSD calculations for the Im-[Co^{III}(corrin)]-CH_3^+ system can be elaborated on by examining the RHF orbitals (displayed in Fig. 5) involved in the largest R_1 and R_2 amplitudes defining the EOM-CCSD wave functions. As shown in Table 3, the S_1 state resulting from the EOM-CCSD calculations has several large contributions from single excitations and some much smaller contributions from double excitations. Closer inspection of the largest excitation amplitudes in the EOM-CCSD description of the S_1 state shows that the main contribution to this state originates from a $\pi/\sigma(d_{z^2})\rightarrow\pi^*$ excitation. The second largest R_1 value represents a $\pi\rightarrow\pi^*$ transition. The remaining singly as well as doubly excited amplitudes contributing to the S_1 state, although smaller than the leading two, have a mixed $d/\pi\rightarrow\pi^*$ character. Taking into account all of these contributions together, we can conclude that the S_1 state of MeCbl resulting from the EOM-CCSD calculations has a predominantly $d/\pi\rightarrow\pi^*$ (i.e., MLCT) character. This MLCT character of the S_1 state is consistent with the assignment based on the independent MC-XQDPT2 calculations.

Unlike in the S_1 case, the EOM-CCSD results for the S_2 and S_3 states do not coincide with the results of the MC-XQDPT2 calculations. Indeed, the EOM-CCSD S_2 state is dominated by the $d_{x^2-y^2}/\sigma_{Corr}/\sigma_{Im}\rightarrow d_{xy}$ + n contributions, and it also has significant contributions that correspond to transfer of an electron from the Co d and corrin σ orbitals to the unoccupied MOs of a similar character. Analogous remarks apply to the EOM-CCSD S_3 state, which also has significant excitations involving the π^* orbital. We can conclude that the S_2 and S_3 states can be characterized as mainly single $d\rightarrow d$ + n transitions in the EOM-CCSD description. Although this particular finding is not consistent with the results obtained with the MC-XQDPT2 approach, it is reassuring that the independent EOM-CCSD and MC-XQDPT2 methodologies agree in the interpretation of the lowest excited S_1 state of MeCbl of interest in this study, which they both classify as a predominantly MLCT $d\rightarrow\pi^*$ or $d/\pi\rightarrow\pi^*$ transition. The S_2 and S_3 states resulting from the EOM-CCSD calculations are considerably higher in energy and, as such, probably do not contribute to the α/β bands, although it would be useful to examine if the incorporation of triple excitations in the EOM-CC calculations could change this conclusion. Unfortunately, we are unable to perform the EOM-CC calculations corrected for triples at this time due to prohibitive computer costs.

Comparison of TD-DFT and ab initio wavefunction-based calculations

The TD-DFT formalism offers a relatively inexpensive approach to electronic excitations in complex molecular systems, but, as pointed out in the Introduction, the results of TD-DFT calculations for cobalamins strongly depend on the choice of the functional. Therefore, selection of the proper functional represents a critical step prior to any extensive investigation directed towards the photochemistry or photophysics of B_{12} cofactors. The recent benchmark analysis of the parent vitamin B_{12} complex provided arguments supporting the superiority of BP86 over the B3LYP functional in terms of its electronically excited states.[66] The question arises whether a similar conclusion applies to MeCbl.

It has previously been noticed that while hybrid functionals overestimate excitation energies, their pure GGA counterparts

Table 4. Orbital composition of the S_1 excited state of Im-[Co^{III}(corrin)]-CH_3^+ resulting from the TD-DFT calculations with different density functionals and basis sets.

	6–31G(d)		6–311++G(d,p)	
Functional[a]	E (eV)	Character	E (eV)	Character
B3LYP (20% HF)	2.65	94% ($\pi + d_{z^2} \rightarrow \pi^*$)	2.68	93% ($\pi + d_{z^2} \rightarrow \pi^*$)
CAM-B3LYP[b]	2.87	22% ($d_{xz} + \pi \rightarrow \pi^* + d_{xy}/d_{z^2}$) + 17% ($\pi + d_{yz} \rightarrow \pi^* + d_{xy}/d_{z^2}$) + 16% ($d_{yz} + \pi \rightarrow \pi^* + d_{xy}/d_{z^2}$) + 15% ($\pi + d_{z^2} \rightarrow \pi^*$)		
BLYP	2.19	71% ($\pi + d_{xz} \rightarrow \pi^*$) + 27% ($d_{xz} + \pi \rightarrow \pi^*$)	2.26	61% ($\pi + d_{xz} \rightarrow \pi^*$) + 8% ($d_{xz} + \pi \rightarrow \pi^*$)
LC-BLYP ($\mu = 0.00$)	2.20	70% ($\pi + d_{xz} \rightarrow \pi^* + d_{yz}$) + 28% ($d_{xz} \rightarrow \pi^* + d_{yz}$)		
LC-BLYP ($\mu = 0.10$)	2.27	50% ($\pi + d_{z^2} \rightarrow \pi^* + d_{yz}$) + 48% ($d_{xz} \rightarrow \pi^* + d_{yz}$)		
MPW1PW91 (25% HF)	2.70	95% ($\pi + d_{z^2} \rightarrow \pi^*$)	2.73	94% ($\pi + d_{z^2} \rightarrow \pi^*$)
MPWPW91	2.19	78% ($\pi + d_{xz} \rightarrow \pi^*$) + 20% ($d_{xz} + \pi \rightarrow \pi^*$)	2.25	69% ($\pi + d_{xz} \rightarrow \pi^*$) + 9% ($d_{xz} + \pi \rightarrow \pi^*$)
TPSSh (10% HF)	2.52	89% ($\pi + d_{z^2} \rightarrow \pi^*$) + 9% ($d_{xz} + \pi \rightarrow \pi^*$)	2.55	93% ($\pi + d_{z^2} \rightarrow \pi^*$) + 4% ($d_{xz} + \pi \rightarrow \pi^*$)
TPSS	2.29	67% ($\pi + d_{xz}/d_{z^2} \rightarrow \pi^*$) + 31% ($d_{xz} + \pi \rightarrow \pi^*$)	2.35	69% ($\pi + d_{xz}/d_{z^2} \rightarrow \pi^*$) + 26% ($d_{xz} + \pi \rightarrow \pi^*$)
BP86	2.18	76% ($\pi + d_{xz}/d_{z^2} \rightarrow \pi^*$) + 22% ($d_{xz} + \pi \rightarrow \pi^*$)	2.25	69% ($\pi + d_{xz}/d_{z^2} \rightarrow \pi^*$) + 29% ($d_{xz} + \pi \rightarrow \pi^*$)

[a] All TD-DFT calculations (apart from LC-BLYP, see below) were performed using the ground-state geometries of Im-[Co^{III}(corrin)]-CH_3^+ optimized with the same functional and basis set as applied in the excited-state calculations. LC-BLYP calculations were performed using the ground-state geometry of Im-[Co^{III}(corrin)]-CH_3^+ optimized with BP86/6–31G(d). [b] The $\alpha = 0.19$, $\beta = 0.46$, and $\mu = 0.33$ parameters, recommended in Ref. [75] and implemented in Gaussian 09, were used in the CAM-B3LYP calculations.

tend to underestimate them.[36,56,57,66] As shown in Table 1, a similar trend is observed when the low-lying excited states of MeCbl are examined, although one also has to point out that the excitation energies obtained with pure functionals, represented in this work by the BLYP, MPWPW91, TPSS, and BP86 approaches, are in much better agreement with the experimentally derived data of Ref. [27] than the excitation energies obtained with hybrid functionals. A comparison of the $S_0 \rightarrow S_1$ excitation energies computed with the hybrid and the corresponding nonhybrid approaches, that is, MPW1PW91 and MPWPW91, B3LYP and BLYP, and TPSSh and TPSS, shows differences of 0.51, 0.46, and 0.23 eV for the respective pairs of functionals. These differences correlate with the amounts of the HF exchange in the hybrid functionals under consideration, which are 25, 20, and 10% for MPW1PW91, B3LYP, and TPSSh, respectively, implying that functionals with smaller fractions of the HF exchange provide a more accurate description of the S_1 state of MeCbl. A comparison of the $S_0 \rightarrow S_1$ excitation energy obtained with the B3LYP functional and its long-range corrected CAM-B3LYP counterpart shows a difference of 0.22 eV, where the lower excitation energy value of 2.65 eV, which itself is considerably higher than the $S_0 \rightarrow S_1$ excitation energies obtained with pure GGAs, is provided by the former functional. The analogous computations using the long-range corrected LC-BLYP method indicate a systematic increase in the excitation energies for larger values of the range separation parameter μ (see Supporting Information Table S2). When μ is close to zero, the LC-BLYP functional approximates its pure exchange-correlation counterpart, while increasing μ produces excitation energies similar to hybrid functionals. Based on the above analysis, we may conclude that by lowering excitation energies, the pure DFT functionals, such as MPWPW91, TPSS, and BP86, work better than the corresponding hybrid approaches when the low-lying excited states of MeCbl are examined. However, the final conclusion regarding the suitability of various functionals for studying electronic properties of MeCbl cannot be based on examining the energetics only. The nature of electronic transitions has to be considered as well, and we discuss this aspect of our calculations next.

When the physical nature of the S_1 state, which the high-level MC-XQDPT2 and EOM-CCSD wavefunction-based methods characterize as an MLCT excitation, is examined with TD-DFT, it becomes clear that the results strongly depend on the applied functional (see Table 4). Indeed, while hybrid functionals support the interpretation in which the S_1 state represents a $\pi \rightarrow \pi^*$ transition localized on corrin, pure GGA, meta-GGA, and range-separated LC-BLYP approaches produce the results which are consistent with an MLCT assignment suggested by MC-XQDPT2 and EOM-CCSD. Before discussing the nature of the S_1 state any further, it is important to emphasize that its character resulting from the TD-DFT calculations is, to a large extent, insensitive to the quality of the basis set. The results based on the smaller 6-31G(d) basis set are virtually identical to those obtained with the larger 6-311++G(d,p) basis (see Table 4), most likely reflecting on the fact that the S_1 state of MeCbl is localized within the corrin macrocycle. Two hybrid functionals under consideration, B3LYP and MPW1PW91, describe the S_1 state as a single HOMO-LUMO excitation (see Table 4 and Supporting Information Tables S7 and S18). The orbital composition of this excitation indicates that contributions from the Co d orbitals are relatively small and that the $S_0 \rightarrow S_1$ transition predicted by hybrid functionals can be characterized as belonging to the corrin $\pi \rightarrow \pi^*$ type. Although similar remarks apply to the TPSSh functional, which describes the S_1 state as a predominantly $\pi/d_{z^2} \rightarrow \pi^*$ transition, one can also see additional contributions involving excitations from HOMO-2, in which the electron density is largely localized on the Co d orbitals with some admixture of the corrin's π orbitals (see Supporting Information Table S12).

The results based on the pure GGA-type functionals (BLYP, MPWPW91, TPSS, and BP86) were found to be very similar in terms of both the energy and the nature of the electronic excitation (Table 4). All four pure functionals used in this study predict significant $\pi/d \rightarrow \pi^*$ (MLCT-like) contributions to the S_1 state of MeCbl. In contrast to hybrid functionals, the $S_0 \rightarrow S_1$

Table 5. The first three excited states of Im-[Co^{III}(corrin)]-CH_3^+ calculated with BP86/6–311++G(d,p).

State	E (eV)[c]	λ (nm)	*f*	Contribution	Transition[a],[b]		Exp (eV)[c]
S_1	2.25	551.4	0.0035	−0.380	115 → 118	29% ($d_{xz} + \pi \rightarrow \pi^*$)	2.22
				0.589	116 → 118	69% ($\pi + d_{xz}/d_{z^2} \rightarrow \pi^*$)	
S_2	2.38	521.4	0.0271	0.150	116 → 119	5% ($\pi + d_{xz}/d_{z^2} \rightarrow d_{xy} + n + \pi^*$)	2.35
				−0.153	116 → 120	5% ($\pi + d_{xz}/d_{z^2} \rightarrow \pi^* + d_{xy}$)	
				0.660	117 → 118	87% ($d_{yz} + \pi \rightarrow \pi^*$)	
S_3	2.50	496.6	0.0565	0.254	114 → 118	13% ($d_{x^2-y^2} \rightarrow \pi^*$)	2.55
				0.532	115 → 118	57% ($d_{xz} + \pi \rightarrow \pi^*$)	
				0.343	116 → 118	24%($\pi + d_{xz}/d_{z^2} \rightarrow \pi^*$)	
				0.116	117 → 120	3% ($d_{yz} + \pi \rightarrow \pi^* + d_{xy}$)	

[a] The isosurface plots of the corresponding MOs are shown in Supporting Information Figure S8. [b] The natural transition orbitals (NTOs) corresponding to the presented electronic transitions are shown in Figure 6. [c]The experimental excitation-energy values reported in Ref. [27] are 17,870, 18,950, and 20,550 cm^{-1}, respectively.

transitions resulting from the GGA-type calculations have a more complex character and originate from HOMO-1→LUMO and HOMO-2→LUMO excitations. The composition of frontier MOs involved in these electronic excitations indicates larger participation of the d orbitals of Co (see Supporting Information Tables S6, S10, S14, and S17). This observation is consistent with the EOM-CCSD calculations, where the S_1 state is dominated by a $\pi/\sigma(d_{z^2}) \rightarrow \pi^*$ transition, with a small admixture of other excitations, particularly those originating from the transitions from the occupied Co d and corrin π orbitals to the unoccupied π^* orbital of the corrin macrocycle (cf. Table 3). In the MC-XQDPT2 calculations, the same state appears as a predominantly d→π^* excitation, with the corrin π occupied orbitals also participating in the transition (see Table 2). Based on the distribution of the electron density among the Co d orbitals, it can be concluded that the d_{z^2} orbital is not the only one that is required for a proper description of the S_1 state. According to both types of the high-level *ab initio* wave-function calculations performed in this study, the $S_0 \rightarrow S_1$ electronic transition involves the Co d orbitals along the axis connecting the two axial ligands of MeCbl. Such a contribution (i.e., $d_{xz} + \pi \rightarrow \pi^*$) is also observed when the results obtained with the pure GGA-type (BLYP, MPWPW91, TPSS, and BP86) functionals are examined. Similarly, when the $S_0 \rightarrow S_1$ excitation is examined using the LC-BLYP approaches, the d_{z^2} and d_{xz} occupied orbitals contribute when $\mu = 0.10$ and 0.20, but when μ is set at zero, the d_{z^2} orbital does not participate in it. Interestingly, the CAM-B3LYP functional introduces significant contributions from the Co d orbitals not only to the occupied but also to the unoccupied MOs participating in the $S_0 \rightarrow S_1$ excitation. This leads to a mixed d/$\pi \rightarrow \pi^*$/d character of the S_1 state. Since the EOM-CCSD calculations clearly indicate that the unoccupied orbitals participating in the lowest excited state of MeCbl are largely corrin-localized (i.e., of the π^* type), and since the MC-XQDPT2 calculations show the contributions from the π^* orbitals localized on corrin to the unoccupied MOs involved in the $S_0 \rightarrow S_1$ transition are larger than the contributions from the Co d orbitals, the results obtained with the CAM-B3LYP functional disagree with both EOM-CCSD and MC-XQDPT2. They are not only inconsistent with an MLCT assignment suggested by the EOM-CCSD and MC-XQDPT2 calculations, but also with a traditional $\pi \rightarrow \pi^*$ description of the $S_0 \rightarrow S_1$ excitation.

The reliability of the MLCT assignment provided by the BP86 and other pure GGA functionals can be further confirmed by considering the nature of the three lowest-energy excited states of MeCbl, as shown in Table 5. According to the BP86 calculations and independent of the basis set used in these calculations, S_1, S_2, and S_3 are close lying states and the $S_0 \rightarrow S_1$ and $S_0 \rightarrow S_3$ transitions involve the same subsets of orbitals. Although the relative contributions from various orbital excitations vary from state to state, both $S_0 \rightarrow S_1$ and $S_0 \rightarrow S_3$ can be characterized as d/$\pi \rightarrow \pi^*$ transitions. A very similar description applies to the S_2 state, which possesses an even larger contribution from the d orbitals of Co. All of this allows us to conclude that not only S_1 but also the next two electronic excitations in MeCbl, which have larger intensities than S_1, share the MLCT character. The MLCT nature of the S_1, S_2, and S_3 states resulting from the use of BP86 and other pure functionals is in good agreement with the MC-XQDPT2 calculations, and there also is a great degree of consistency in the characterization of the S_1 state as an MLCT transition by pure GGAs and EOM-CCSD. It is, therefore, quite certain that the lowest-energy excitations in MeCbl are MLCT transitions.

Additional insights into the nature of the three lowest-energy excited states of MeCbl can be obtained through the use of the natural transition orbitals (NTOs) of Martin,[119] which are shown for the Im-[Co^{III}(corrin)]-CH_3^+ model of MeCbl in Figure 6. According to the NTO analysis, the S_1 state can be described as an out-of-phase $d_{z^2} - d_{xz}$ combination of the Co d orbitals, whereas S_3 is an in-phase $d_{z^2} + d_{xz}$ combination. This explains why the intensity of the S_1 state is much lower in comparison to S_3; the transition dipole moments cancel out in the former case and add up in the case of the latter excitation. The nature of the NTOs shown in Figure 6 also reveals that none of the low-lying excitations in MeCbl can be classified as pure MLCT or pure $\pi \rightarrow \pi^*$ transitions. These transitions always appear together and, due to the low symmetry of the corrin ligand, they cannot be completely separated. Thus, to understand the relative magnitudes of the MLCT and $\pi \rightarrow \pi^*$ contributions to the low-lying excited states of MeCbl, we calculated the electron density differences between S_0 and S_1, S_0 and S_2, and S_0 and S_3 using the BP86/6-311++G(d,p) approach (see Fig. 7). A direct inspection of these electron density differences corroborates our main conclusion that the S_1 state of

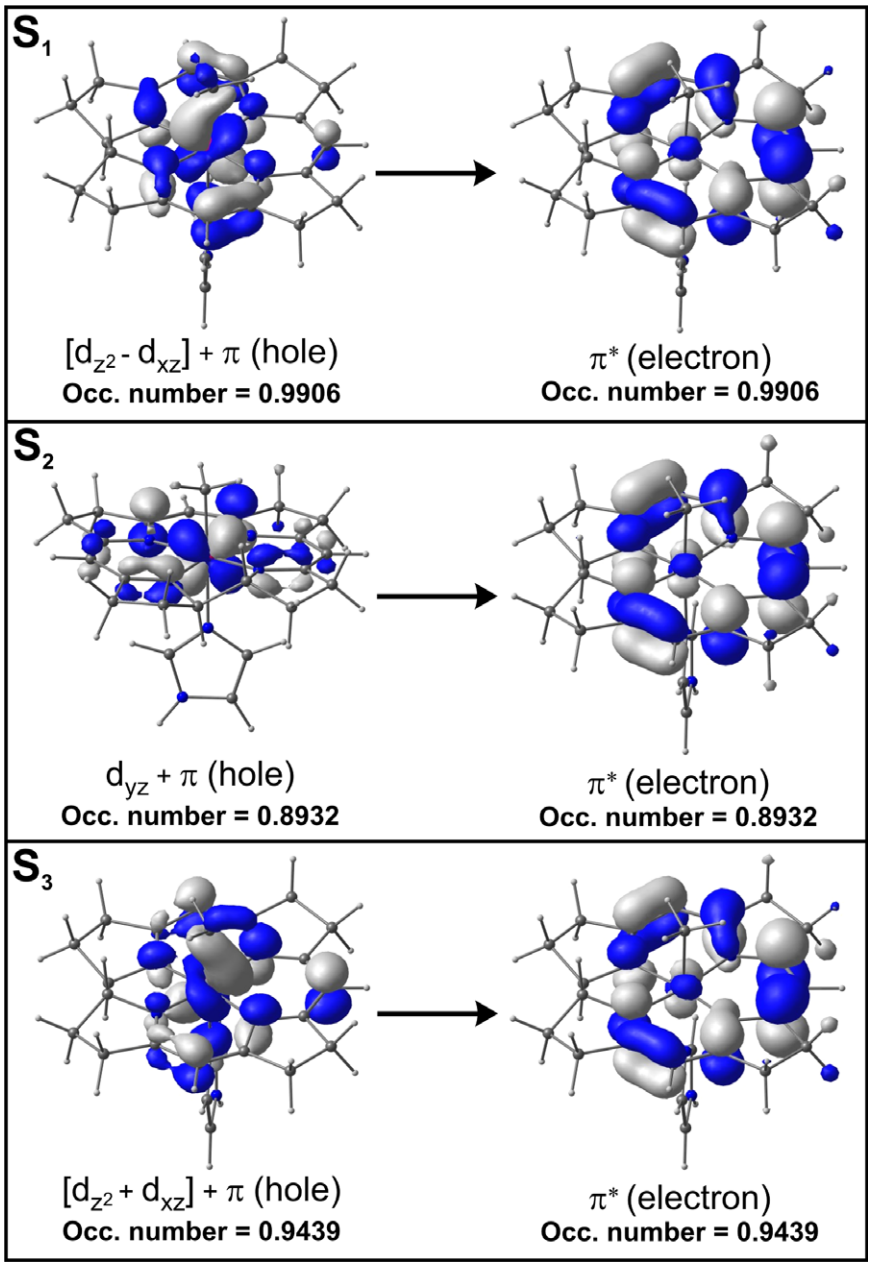

Figure 6. Natural transition orbitals (NTOs) describing the three lowest singlet excited states for the Im-[Co^{III}(corrin)]-CH_3^+ model complex. Results obtained from the TD-DFT/BP86/6-311++G(d,p) calculations. [Color figure can be viewed in the online issue, which is available at wileyonlinelibrary.com.]

MeCbl has indeed an MLCT character. There is a visible outflow of the electron density from the Co atom and along the N_{Im}—Co—C_{Me} axis, and there also is a noticeable electron density inflow toward the corrin ring. Similar decreases of the electron density on Co with concurrent density increases on corrin are also observed for the $S_0 \rightarrow S_2$ and $S_0 \rightarrow S_3$ transitions (see Fig. 7), confirming the d/$\pi \rightarrow \pi^*$ nature of the low-lying excited states of MeCbl postulated in this study.

Adiabatic nature of the S_1 transition

Up to this point, we have mainly focused on comparing the results obtained with the two high-level *ab initio* wave-function methods with those obtained with TD-DFT to understand the nature of the low-lying excited states of the Im-[Co^{III}(corrin)]-CH_3^+ complex. Relying on the overall agreement between the MC-XQDPT2 and EOM-CCSD results and based on the reasonable agreement between the TD-DFT calculations using pure GGAs and the high-level *ab initio* data, the lowest-energy S_1 state has been characterized as an MLCT-type transition. The MC-XQDPT2 and EOM-CCSD $S_0 \rightarrow S_1$ excitation energies of 2.48 and 2.65 eV, respectively, are in good agreement with the experimental value of 2.22 eV (see Table 1). The nonhybrid functionals, including BLYP, MPWPW91, TPSS, BP86, and LC-BLYP ($\mu = 0.00$ or 0.10), provide a description which is consistent with the S_1 state being an MLCT transition. The corresponding excitation energies of 2.19, 2.19, 2.29, 2.18, and 2.20 or 2.27 eV, respectively, obtained with the 6-31G(d) basis set are remarkably close to the experimental

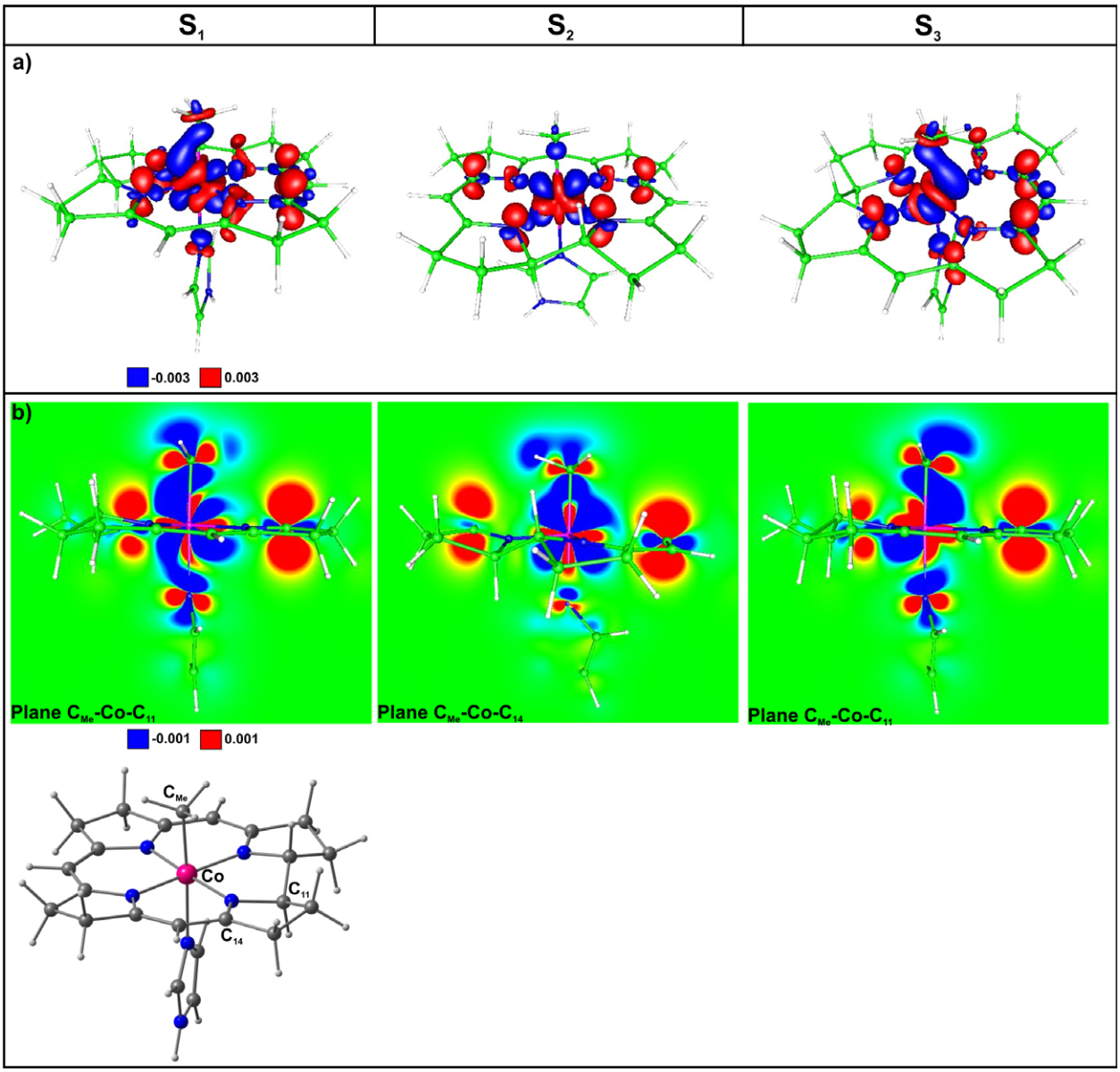

Figure 7. Electron density differences between the S_0 and S_1, S_0 and S_2, and S_0 and S_3 states for the Im-[Co^{III}(corrin)]-CH_3^+ model complex: a) isosurface plot value of 0.003 and b) cross-section contour plot along the axial bonding. Results obtained from the TD-DFT/BP86/6-311++G(d,p) calculations. [Color figure can be viewed in the online issue, which is available at wileyonlinelibrary.com.]

value of 2.22 eV (see Table 1), and the use of larger basis sets, such as 6-311G(d,p) and 6-311++G(d,p), has virtually no effect on these findings (cf. Table 5 and Supporting Information Tables S22 and S23). Based on the energetics and the physical nature of the electronic transitions in MeCbl obtained with different methods, as discussed above, the present study supports the MLCT interpretation of the lowest S_1 state rather than the traditional interpretation of this state as a $\pi\rightarrow\pi^*$ transition localized on corrin.

To provide a more complete understanding of the $S_0\rightarrow S_1$ transition, we also examined the mechanism governing this transition. In the lowest order description, the Abs, CD, and MCD spectroscopies are guided by the Franck–Condon (FC) principle, which assumes that the nuclear configuration does not change upon electronic excitation. In contrast, TAS explores the photoproducts at different time delays. The absorbance at a particular wavelength (or range of wavelengths) is measured as a function of time after excitation by a flash of light. Thus, in examining the results of TAS experiments, it is more appropriate to discuss the adiabatic nature of the $S_0\rightarrow S_1$ transition, focusing on the electronic properties of MeCbl in terms of the photo-induced geometrical changes.

Since one can expect that the most significant changes in the electronic structure of the S_1 state of MeCbl are associated with the photo-induced geometrical changes in additional axial ligands,[59] the additional calculations evaluating additional energy changes in response to the variations of the Co—C_{Me} and Co—N_{Im} distances were performed. For each point on the two-dimensional potential energy surface (PES) cut defined by fixed Co—C_{Me} and Co—N_{Im} distances, the ground-state

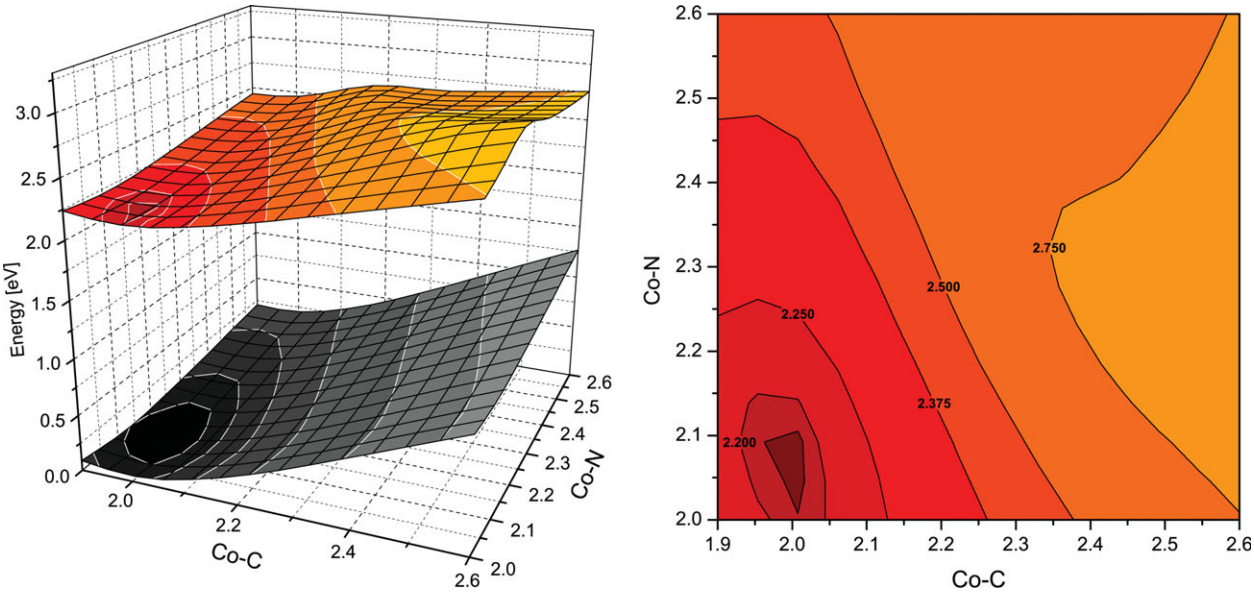

Figure 8. Left panel—potential energy surfaces of the S_0 and S_1 states resulting from the BP86 and TD-DFT/BP86/6-31G(d) calculations plotted as a function of axial bond lengths (in Å). Right panel—vertical projection of the potential energy surface of the S_1 state.

structure of Im-[Co^{III}(corrin)]-CH_3^+ was reoptimized. The Co—C_{Me} and Co—N_{Im} distances were varied between 1.9 and 2.6 Å, with a step of 0.1 Å, in the former case and from 2.0 to 2.6 Å, with a step of 0.1 Å as well, in the latter case, allowing for the full relaxation of remaining geometrical parameters. Taking into account the fact that the character of the S_1 state is not significantly affected by the basis set, only the smaller 6-31G(d) basis set was used in these calculations. The two-dimensional PES cuts of the S_0 and S_1 states along the Co—C_{Me} and Co—N_{Im} coordinates, resulting from the BP86/6-31G(d) and subsequent TD-DFT/BP86/6-31G(d) calculations, are shown in Figure 8. Considering the fact that upon electronic excitation the geometry of MeCbl might relax to another stable structure (as in the case of CNCbl[120]), the presence of additional minima on the PES of the S_1 state might lead to questions about the characterization of the $S_0 \rightarrow S_1$ transition as an MLCT excitation based on the vertical excitations only. However, careful inspection of Figure 8 shows that there is only one minimum on the PES of the S_1 state. Compared to the ground-state equilibrium geometry of the Im-[Co^{III}(corrin)]-CH_3^+ system, the minimum on the S_1 PES is only slightly shifted toward shorter Co—N_{Im} distances (from 2.15 Å in the case of S_0 state to about 2.05 Å in the S_1 case) and almost unchanged with respect to the Co—C_{Me} bond-length (which is 1.98 Å for the S_0 state and 2.00 Å for the S_1 state). These small geometrical changes upon the electronic excitation support the validity of the previously discussed MLCT interpretation of the S_1 state, which has been based on the vertical $S_0 \rightarrow S_1$ excitation calculated using several pure and range-separated DFT functionals, EOM-CCSD, and MC-XQDPT2.

To reconfirm the MLCT nature of the $S_0 \rightarrow S_1$ transition in yet another way, the geometry of the Im-[Co^{III}(corrin)]-CH_3^+ complex in its S_1 state was also fully reoptimized at the TD-DFT/BP86/6-31G(d) level. Only small structural changes between the S_0 and S_1 states, mostly in the axial ligands, were observed (Fig. 9). The $S_0 \rightarrow S_1$ excitation resulted in the 0.015 Å elongation of the Co—C_{Me} bond, the 0.092 Å shortening of the Co—N_{Im} bond, and the 12.5° change in the N_{Im}—Co—C_{Me} angle value. The subsequent analysis of MOs participating in the lowest electronic excitation showed once again that the S_1 state is dominated by the d/$\pi \rightarrow \pi^*$ MLCT excitations (see Fig. 10), in perfect agreement with the TAS experiments of Sension et al.[42,44,46,50]

Summary and Conclusions

The goal of the present study was to provide insights into the nature of the S_1 state of the MeCbl cofactor, which was previously characterized as either the $\pi \rightarrow \pi^*$ excitation localized on corrin[21,22,27,30] or the MLCT excitation.[42,44,46,50] To resolve the existing controversy, we performed high-level *ab initio* calculations, including the MC-XQDPT2 and EOM-CCSD wave-function-based methods, and several TD-DFT calculations using the hybrid (B3LYP, MPW1PW91, TPSSh), GGA-type (BP86, BLYP, MPWPW91), meta-GGA (TPSS), and range-separated (CAM-B3LYP and LC-BLYP) functionals. We have demonstrated that the MC-XQDPT2 and EOM-CCSD approaches provide a consistent description of the S_1 state as an MLCT transition, in agreement with the TAS experiments.[42,44,46,50] In contrast to the high-level wave-function approaches, the TD-DFT results vary significantly depending on the applied functional. The commonly used hybrid functionals, including B3LYP, MPW1PW91, and TPSS-h, suggest a predominantly $\pi \rightarrow \pi^*$ character of the $S_0 \rightarrow S_1$ transition, as opposed to the MLCT interpretation resulting from the MC-XQDPT2 and EOM-CCSD calculations. Conversely, the GGA-type (BP86, BLYP, and MPWPW91), meta-GGA (TPSS), and range-separated (LC-BLYP) functionals characterize it as a predominantly MLCT, d/$\pi \rightarrow \pi^*$, excitation, in agreement with the MC-XQDPT2 and EOM-CCSD calculations. Thus, the previous assignments of the low-lying excitations of

MeCbl derived from the experimental Abs, CD, and MCD spectra coupled with the theoretical analysis based on the functionals other than GGAs[27,30] may require revision. Clearly, additional experimental and theoretical work is needed to fully understand the nature of the electronically excited states of the MeCbl cofactor. However, in view of the high-level *ab initio* calculations reported in this work and the recent TAS studies,[42,44,46,50] it is reasonable to assume that the S_1 state of MeCbl is an MLCT transition.

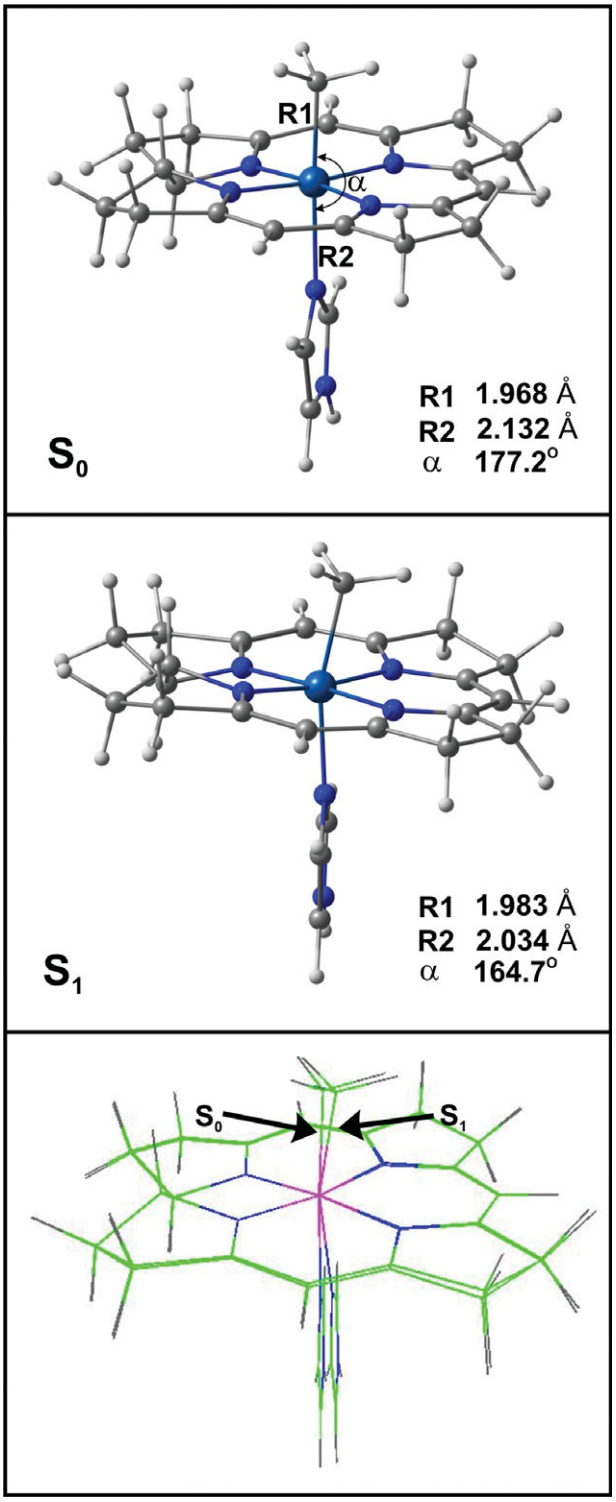

Figure 9. A comparison of the BP86/6-31G(d)-optimized geometries of the ground (top) and first excited (middle) state of Im-[Co^{III}(corrin)]-CH_3^+, along with the alignment of their structures (bottom).

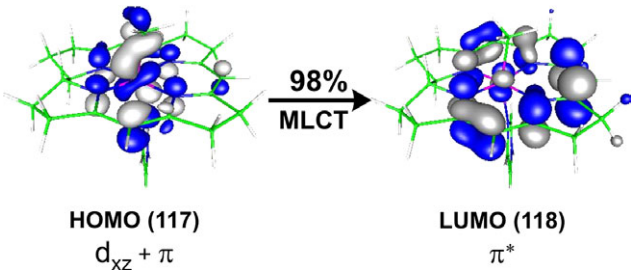

Figure 10. The isosurface plots of dominant MOs corresponding to the first electronic transition ($S_0 \rightarrow S_1$) of Im-[Co^{III}(corrin)]-CH_3^+ at the TD-DFT/BP86/6-31G(d)-optimized geometry of the S_1 excited state. [Color figure can be viewed in the online issue, which is available at wileyonlinelibrary.com.]

Acknowledgments

The authors would like to acknowledge the Cardinal Research Cluster (Supercomputing Facilities at the University of Louisville) for providing computational resources. The TURBOMOLE calculations were carried out in the Academic Computer Centre CYFRONET of the University of Science and Technology in Cracow, ACC CYFRONET AGH, Kraków, Poland, http://www.cyfronet.pl, under grant No. MNiSW/SGI3700/USląski/111/2007 and MNiSW/IBM_BC_HS21/USląski/111/2007.

Keywords: excited states · B_{12} cofactors · complete active space self-consistent field · second-order multiconfigurational quasi-degenerate perturbation theory · equation-of-motion coupled-cluster singles and doubles · time-dependent density functional theory · methylcobalamin

How to cite this article: K. Kornobis, N. Kumar, P. Lodowski, M. Jaworska, P. Piecuch, J. J. Lutz, B. M. Wong, P. M. Kozlowski, *J. Comput. Chem.* **2013,** *34,* 987–1004. DOI: 10.1002/jcc.23204

Additional Supporting Information may be found in the online version of this article.

[1] D. Dolphin, Ed. B_{12}; Wiley-Interscience, New York, **1982**.
[2] R. Banerjee, *Chem. Biol.* **1997**, *4,* 175.
[3] M. L. Ludwig, R. G. Matthews, *Annu. Rev. Biochem.* **1997**, *66,* 269.
[4] B. Kräutler, D. Arigoni, B. T. Golding, Eds. Vitamin B_{12} and B_{12} Proteins; Wiley-VCH: New York, **1998**.
[5] L. G. Marzilli, In Bioinorganic Catalysis; J. Reedijk, E. Bouwman, Eds.; Marcel Dekker: New York, **1999**; pp. 423–468.
[6] R. Banerjee, Chemistry and Biochemistry of B_{12}; John Wiley & Sons: New York, **1999**.
[7] T. Toraya, *Cell. Mol. Life Sci.* **2000**, *57,* 106.
[8] R. Banerjee, *Biochemistry* **2001**, *40,* 6191.
[9] R. G. Matthews, *Acc. Chem. Res.* **2001**, *34,* 681.
[10] R. Banerjee, S. W. Ragsdale, *Annu. Rev. Biochem.* **2003**, *72,* 209.
[11] R. Banerjee, *Chem. Rev.* **2003**, *103,* 2083.
[12] T. Toraya, *Chem. Rev.* **2003**, *103,* 2095.
[13] K. L. Brown, *Chem. Rev.* **2005**, *105,* 2075.
[14] L. Randaccio, S. Geremia, G. Nardin, J. Wuerges, *Coord. Chem. Rev.* **2006**, *250,* 1332.

[15] L. Randaccio, S. Geremia, J. Wuerges, *J. Organomet. Chem.* **2007**, *692,* 1198.
[16] R. G. Matthews, M. Koutmos, S. Datta, *Curr. Opin. Struct. Biol.* **2008**, *18,* 658.
[17] L. Randaccio, S. Geremia, N. Demitri, J. Wuerges, *Trends Inorg. Chem.* **2009**, *11,* 1.
[18] R. G. Matthews, In Metal Ions in Life Sciences, Vol. *6; A. Sigel, H. Sigel, R. K. O. Sigel, Eds.; Royal Society of Chemistry: Cambridge, UK,* **2009**; pp. 53–114.
[19] L. Randaccio, S. Geremia, N. Demitri, J. Wuerges, *Molecules* **2010**, *15,* 3228.
[20] R. A. Firth, H. A. O. Hill, J. M. Pratt, R. J. P. Williams, W. R. Jacson, *Biochemistry* **1967**, *6,* 2178.
[21] C. Giannotti, In B_{12}, Chapter 11; D. Dolphin, Ed., Wiley-Interscience: New York, **1982**, pp. 393–430.
[22] J. M. Pratt, In Chemistry and Biochemistry of B_{12}, Chapter 5; R. Banerjee, Ed.; John Wiley & Sons: New York, **1999**; pp. 113–164.
[23] P. Day, *Theor. Chim. Acta,* **1967**, *7,* 328.
[24] P. Day, *Coord. Chem. Rev.,* **1967**, *2,* 109.
[25] P. O. Offenhartz, B. H. Offenhartz, M. M. Fung, *J. Am. Chem. Soc.* **1970**, *92,* 2966.
[26] J. I. Toohey, *Proc. Natl. Acad. Sci. USA* **1965**, *54,* 934.
[27] T. R. Stich, A. J. Brooks, N. R. Buan, T. C. Brunold, *J. Am. Chem. Soc.* **2003**, *125,* 5897.
[28] T. R. Stich, N. R. Buan, T. C. Brunold, *J. Am. Chem. Soc.* **2004**, *126,* 9735.
[29] M. D. Liptak, T. C. Brunold, *J. Am. Chem. Soc.* **2006**, *128,* 9144.
[30] T. C. Brunold, K. S. Conrad, M. D. Liptak, K. Park, *Coord. Chem. Rev.* **2009**, *253,* 779.
[31] E. Runge, E. K. U. Gross, *Phys. Rev. Lett.* **1984**, *52,* 997.
[32] E. J. Baerends, G. Ricciardi, A. Rosa, S. J. A. van Gisergen, *Coord. Chem. Rev.* **2002**, *230,* 5.
[33] A. Rosa, G. Ricciardi, O. Gritsenko, E. J. Baerends, *Struct. Bond.* **2004**, *112,* 49.
[34] A. Dreuw, M. Head-Gordon, *Chem. Rev.* **2005**, *105,* 4009.
[35] A. Dreuw, *ChemPhysChem* **2006**, *7,* 2259.
[36] T. Andruniów, P. M. Kozlowski, M. Z. Zgierski, *J. Chem. Phys.* **2001**, *115,* 7522.
[37] M. Jaworska, P. Lodowski, *J. Mol. Struct. (THEOCHEM)* **2003**, *631,* 209.
[38] M. Jaworska, G. Kozibut, P. Lodowski, *J. Phys. Chem. A* **2005**, *107,* 1339.
[39] A. D. Becke, *J. Chem. Phys.,* **1993**, *98,* 5648.
[40] C. Lee, W. Yang, R. G. Parr, *Phys. Rev. B,* **1988**, *37,* 785.
[41] P. E. M. Siegbahn, T. Borowski, *Acc. Chem. Res.,* **2006**, *39,* 729.
[42] L. A. Walker, II, J. T. Jarrett, N. A. Anderson, S. H. Pullen, R. G. Matthews, R. J. Sension, *J. Am. Chem. Soc.* **1998**, *120,* 3597.
[43] L. A. Walker, II, J. J. Shiang, N. A. Anderson, S. H. Pullen, R. J. Sension, *J. Am. Chem. Soc.* **1998**, *120,* 7286.
[44] J. J. Shiang, L. A. Walker, II, N. A. Anderson, A. G. Cole, R. J. Sension, *J. Phys. Chem. B* **1999**, *103,* 10532.
[45] L. M. Yoder, A. G. Cole, L. A. Walker, II, R. J. Sension, *J. Phys. Chem. B* **2001**, *105,* 12180.
[46] A. G. Cole, L. M. Yoder, J. J. Shiang, N. A. Anderson, L. A. Walker, II, M. M. Banaszak Holl, R. J. Sension, *J. Am. Chem. Soc.* **2002**, *124,* 434.
[47] R. J. Sension, D. A. Harris, A. Stickrath, A. G. Cole, C. C. Fox, E. N. G. Marsh, *J. Phys. Chem. B* **2005**, *109,* 18146.
[48] R. J. Sension, D. A. Harris, A. G. Cole, *J. Phys. Chem. B* **2005**, *109,* 21954.
[49] J. J. Shiang, A. G. Cole, R. J. Sension, K. Hang, Y. Weng, J. S. Trommel, L. G. Marzilli, T. Lian, N. A. Anderson, *J. Am. Chem. Soc.* **2006**, *128,* 801.
[50] D. A. Harris, A. B. Stickrath, E. C. Carroll, R. J. Sension, *J. Am. Chem. Soc.* **2007**, *129,* 7578.
[51] J. Peng, K. C. Tang, K. McLoughlin, Y. Yang, D. Forgach, R. J. Sension, *J. Phys. Chem. B* **2010**, *114,* 12398.
[52] K. P. Jensen, U. Ryde, *J. Phys. Chem. A* **2003**, *107,* 7539.
[53] J. Kuta, S. Patchkovskii, M. Z. Zgierski, P. M. Kozlowski, *J. Comput. Chem.* **2006**, *27,* 1429.
[54] K. Jensen, U. Ryde, *Coord. Chem. Rev.* **2009**, *253,* 769.
[55] P. M. Kozlowski, M. Kumar, P. Piecuch, W. Li, N. P. Bauman, J. A. Hansen, P. Lodowski, M. Jaworska, *J. Chem. Theory Comput.* **2012**, *8,* 1870.
[56] T. Andruniów, M. Jaworska, P. Lodowski, M. Z. Zgierski, R. Dreos, L. Randaccio, P. M. Kozlowski, *J. Chem. Phys.* **2008**, *129,* 85101.
[57] T. Andruniów, M. Jaworska, P. Lodowski, M. Z. Zgierski, R. Dreos, L. Randaccio, P. M. Kozlowski, *J. Chem. Phys.* **2009**, *131,* 105105.
[58] M. Jaworska, P. Lodowski, T. Andruniów, P. M. Kozlowski, *J. Phys. Chem. B (Letter)* **2007**, *111,* 2419.
[59] P. Lodowski, M. Jaworska, T. Andruniów, M. Kumar, P. M. Kozlowski, *J. Phys. Chem. B* **2009**, *113,* 6898.
[60] A. D. Becke, *Phys. Rev. A* **1988**, *38,* 3098.
[61] J. P. Perdew, *Phys. Rev. B* **1986**, *33,* 8822.
[62] J. Kuta, J. Wuerges, L. Randaccio, P. M. Kozlowski, *J. Phys. Chem. A* **2009**, *113,* 11604.
[63] H. Solheim, K. Kornobis, K. Ruud, P. M. Kozlowski, *J. Phys. Chem. B,* **2011**, *115,* 737.
[64] H. Nakano, *J. Chem. Phys.* **1993**, *99,* 7983.
[65] K. Andersson, P. A. Malmqvist, B. O. Roos, A. J. Sadlej, K. Wolinski, *J. Phys. Chem.* **1990**, *94,* 5483.
[66] K. Kornobis, N. Kumar, B. Wong, P. Lodowski, M. Jaworska, T. Andruniów, K. Ruud, P. M. Kozlowski, *J. Phys. Chem. A* **2011**, *115,* 1280.
[67] J. Geertsen, M. Rittby, R. J. Bartlett, *Chem. Phys. Lett.* **1989**, *164,* 57.
[68] J. F. Stanton, R. J. Bartlett, *J. Chem. Phys.* **1993**, *98,* 7029.
[69] H. Iikura, T. Tsuneda, T. Yanai, K. Hirao, *J. Chem. Phys.* **2001**, *115,* 3540.
[70] C. Adamo, V. Barone, *J. Chem. Phys.* **1998**, *108,* 664.
[71] V. N. Staroverov, G. E. Scuseria, J. Tao, J. P. Perdew, *J. Chem. Phys.* **2003**, *119,* 12129.
[72] A. D. Becke, *Phys. Rev. A,* **1988**, *38,* 3098.
[73] J. P. Perdew, K. Burke, Y. Wang, *Phys. Rev. B* **1996**, *54,* 16533.
[74] J. Tao, J. P. Perdew, V. N. Staroverov, G. E. Scuseria, *Phys. Rev. Lett.* **2003**, *91,* 146401.
[75] T. Yanai, D. P. Tew, N. C. Handy, *Chem. Phys. Lett.* **2004**, *393,* 51.
[76] J. P. Perdew, J. A. Chevary, S. H. Vosko, K. A. Jackson, M. R. Pederson, D. J. Singh, C. Fiolhais, *Phys. Rev. B* **1992**, *46,* 6671.
[77] B. M. Wong, J. G. Cordaro, *J. Chem. Phys.* **2008**, *129,* 214703.
[78] B. M. Wong, M. Piacenza, F. Della Sala, *Phys. Chem. Chem. Phys.* **2009**, *11,* 4498.
[79] B. M. Wong, T. H. Hsieh, *J. Chem. Theory Comput.* **2010**, *6,* 3704.
[80] C. Rovira, P. M. Kozlowski, *J. Phys. Chem. B* **2007**, *111,* 3251.
[81] L. Randaccio, M. Furlan, S. Geremia, M. Slouf, I. Srnova, D. Toffoli, *Inorg. Chem.* **2000**, *39,* 3403.
[82] M. Fasching, W. Schmidt, B. Kräutler, E. Stupperich, A. Schmidt, C. Kratky, *Helv. Chim. Acta* **2000**, *83,* 2295.
[83] A. A. Granovsky, Firefly version 7.1.G, http://classic.chem.msu.su/gran/firefly/index.html
[84] H. Koch, P. Jørgensen, *J. Chem. Phys.* **1990**, *93,* 3333.
[85] H. Koch, H. J. Aa. Jensen, P. Jørgensen, T. Helgaker, *J. Chem. Phys.* **1990**, *93,* 3345.
[86] J. Gauss, In Encyclopedia of Computational Chemistry, Vol. *1; P. v. R. Schleyer, N. L. Allinger, T. Clark, J. Gasteiger, P. A. Kollman, H. F. Schaefer, III, P. R. Schreiner, Eds.; Wiley: Chichester, UK,* **1998**; pp. 615–636.
[87] R. J. Bartlett, M. Musiał, *Rev. Mod. Phys.* **2007**, *79,* 291.
[88] P. Piecuch, M. Włoch, M. Lodriguito, J. R. Gour, In Progress in Theoretical Chemistry and Physics, Vol. *15; Recent Advances in the Theory of Chemical and Physical Systems; J. -P. Julien, J. Maruani, D. Mayou, S. Wilson, G. Delgado-Barrio, Eds.; Springer: Dordrecht,* **2006**; pp. 45–106.
[89] M. Nooijen, R. J. Bartlett, *J. Chem. Phys.* **1998**, *106,* 6449.
[90] S. R. Gwaltey, R. J. Bartlett, *J. Chem. Phys.* **1998**, *108,* 6790.
[91] S. Coussan, Y. Ferro, A. Trivella, P. Roubin, R. Wieczorek, C. Manca, P. Piecuch, K. Kowalski, M. Włoch, S. A. Kucharski, M. Musiał, *J. Phys. Chem. A* **2006**, *110,* 3920.
[92] K. Kowalski, S. Krishnamoorthy, O. Villa, J. R. Hammond, N. Govind, *J. Chem. Phys.* **2010**, *132,* 154103.
[93] G. Fradelos, J. J. Lutz, T. A. Wesołowski, P. Piecuch, M. Włoch, *J. Chem. Theor. Comput.* **2011**, *7,* 1647.
[94] G. D. Purvis III, R. J. Bartlett, *J. Chem. Phys.* **1982**, *76,* 1910.
[95] J. M. Cullen, M. C. Zerner, *J. Chem. Phys.* **1982**, *77,* 4088.
[96] G. E. Scuseria, A. C. Scheiner, T. J. Lee, J. E. Rice, H. F. Schaefer III, *J. Chem. Phys.* **1987**, *86,* 2881.
[97] P. Piecuch, J. Paldus, *Int. J. Quantum Chem.* **1989**, *36,* 429.
[98] K. Kowalski, P. Piecuch, *J. Chem. Phys.* **2004**, *120,* 1715.

[99] P. Piecuch, S. A. Kucharski, K. Kowalski, M. Musiał, *Comput. Phys. Commun.* **2002**, *149,* 71.
[100] M. W. Schmidt, K. K. Baldridge, J. A. Boatz, S. T. Elbert, M. S. Gordon, J. H. Jensen, S. Koseki, N. Matsunaga, K. A. Nguyen, S. J. Su, T. L. Windus, M. Dupuis, J. A. Montgomery, *J. Comput. Chem.* **1993**, *14,* 1347.
[101] M. S. Gordon, M. W. Schmidt, In Theory and Applications of Computational Chemistry: The First Forty Years; C. E. Dykstra, G. Frenking, K. S. Kim, G. E. Scuseria, Eds.; Elsevier: Amsterdam, **2005**; pp. 1167–1190.
[102] Gaussian 09, Revision A.1, M. J. Frisch, G. W. Trucks, H. B. Schlegel, G. E. Scuseria, M. A. Robb, J. R. Cheeseman, G. Scalmani, V. Barone, B. Mennucci, G. A. Petersson, H. Nakatsuji, M. Caricato, X. Li, H. P. Hratchian, A. F. Izmaylov, J. Bloino, G. Zheng, J. L. Sonnenberg, M. Hada, M. Ehara, K. Toyota, R. Fukuda, J. Hasegawa, M. Ishida, T. Nakajima, Y. Honda, O. Kitao, H. Nakai, T. Vreven, J. A. Montgomery, Jr., J. E. Peralta, F. Ogliaro, M. Bearpark, J. J. Heyd, E. Brothers, K. N. Kudin, V. N. Staroverov, R. Kobayashi, J. Normand, K. Raghavachari, A. Rendell, J. C. Burant, S. S. Iyengar, J. Tomasi, M. Cossi, N. Rega, N. J. Millam, M. Klene, J. E. Knox, J. B. Cross, V. Bakken, C. Adamo, J. Jaramillo, R. Gomperts, R. E. Stratmann, O. Yazyev, A. J. Austin, R. Cammi, C. Pomelli, J. W. Ochterski, R. L. Martin, K. Morokuma, V. G. Zakrzewski, G. A. Voth, P. Salvador, J. J. Dannenberg, S. Dapprich, A. D. Daniels, Ö. Farkas, J. B. Foresman, J. V. Ortiz, J. Cioslowski, D. J. Fox, Gaussian, Inc., Wallingford, CT, **2009**.
[103] (a) R. Ahlrichs, M. Bär, M. Häser, H. Horn, C. Kölmel, *Chem. Phys. Lett.* **1989**, *162,* 165; (b) O. Treutler, R. Ahlrichs, *J. Chem. Phys.* **1995**, *102,* 346; (c) F. Furche, R. Ahlrichs, *J. Chem. Phys.* **2002**, *117,* 7433; (d) F. Furche, D. Rappoport, In Theoretical and Computational Chemistry, Vol. *16; M. Olivucci, Ed.; Elsevier, Amsterdam,* **2005**; (e) TURBOMOLE has been designed by the Quantum Chemistry Group, University of Karlsruhe, Germany, since 1988. The following members of the group have made contributions: Reinhart Ahlrichs, Michael Bär, Hans-Peter Baron, Rüdiger Bauernschmitt, Stephan Böcker, Nathan Crawford, Peter Deglmann, Michael Ehrig, Karin Eichkorn, Simon Elliott, Filipp Furche, Frank Haase, Marco Häser, Christof Hättig, Arnim Hellweg, Hans Horn, Christian Huber, Uwe Huniar, Marco Kattannek, Andreas Köhn, Christoph Kölmel, Markus Kollwitz, Klaus May, Paola Nava, Christian Ochsenfeld, Holger Öhm, Holger Patzelt, Dmitrij Rappoport, Oliver Rubner, Ansgar Schäfer, Uwe Schneider, Marek Sierka, Oliver Treutler, Barbara Unterreiner, Malte von Arnim, Florian Weigend, Patrick Weis, and Horst Weiss, available at: http://www.turbomole.com
[104] S. Dong, R. Padmakumar, R. Banerjee, T. G. Spiro, *Inorg. Chem. Acta* **1998**, *270,* 392.
[105] B. O. Roos, In Ab Initio Methods in Quantum Chem.-II, Chapter 69, K. P. Lawley, ed.; Wiley: New York, **1987**, p. 399.
[106] B. O. Roos, K. Andersson, M. P. Fülscher, P. -Å. Malmqvist, L. Serrano Andrés, K. Pierloot, M. Merchán, In Advances in Chemical Physics: New Methods in Computational Quantum Mechanics, Vol. *93; I. Prigogine, S. A. Rice, Eds.; Wiley: New York,* **1996**; pp. 219–332.
[107] M. W. Schmidt, M. S. Gordon, *Annu. Rev. Phys. Chem.* **1998**, *49,* 233.
[108] K. Pierloot, In Computational Photochemistry, Vol. *16; M. Olivucci, Ed., Elsevier: Amsterdam,* **2005**; pp. 279–315.
[109] K. P. Jensen, *J. Phys. Chem. B* **2005**, *109,* 10505.
[110] B. O. Roos, V. Veryazov, J. Conradie, P. R. Taylor, A. Ghosh, *J. Phys. Chem. B* **2008**, *112,* 14099.
[111] N. Kumar, M. Jaworska, P. Lodowski, M. Kumar, P. M. Kozlowski, *J. Phys. Chem. B* **2011**, *115,* 6722.
[112] N. Kumar, M. Alfonso-Prieto, C. Rovira, M. Jaworska, P. Lodowski, P. M. Kozlowski, *J. Chem. Theory Comput.* **2011**, *7,* 1541.
[113] H. Nakatsuji, *Chem. Phys. Lett.* **1978**, *59,* 362.
[114] H. Nakatsuji, *Chem. Phys. Lett.* **1979**, *67,* 329.
[115] H. Nakatsuji, *Chem. Phys. Lett.* **1979**, *67,* 334.
[116] J. Hasegawa, M. Hada, M. Nonoguchi, H. Nakatsuji, *Chem. Phys. Lett.* **1996**, *250,* 159.
[117] T. Miyahara, H. Nakatsuji, J. Hasegawa, A. Osuka, N. Aratani, A. Tsuda, *J. Chem. Phys.* **2002**, *117,* 11196.
[118] P. D. Fan, M. Valiev, K. Kowalski, *Chem. Phys. Lett.* **2008**, *458,* 205.
[119] R. L. Martin, *J. Chem. Phys.* **2003**, *118,* 4775.
[120] P. Lodowski, M. Jaworska, K. Kornobis, T. Andruniów, P. M. Kozlowski, *J. Phys. Chem. B* **2011**, *115,* 13304.

Received: 6 July 2012
Revised: 25 October 2012
Accepted: 19 November 2012
Published online on 19 January 2013